Supporting Information

Highly stable fluorescent coordination polymer materials for the ultrafast detection of nitrofurans in aqueous medium at ppb level

Alokananda Chanda and Sanjay K. Mandal*

Department of Chemical Sciences, Indian Institute of Science Education and Research Mohali, Mohali, Punjab 140306, India

*Author for correspondence:

Prof. Sanjay K. Mandal

E-mail: sanjaymandal@iisermohali.ac.in

Table of Contents

Physical measurements. FTIR spectra were recorded in the 4000 cm^{-1} to 400 cm^{-1} range on a Bruker laser class spectrometer with samples being prepared as KBr pellets. Elemental analysis (C, H, N) was carried out using a Thermo Finnigan analyzer at IIT Bombay. Powder X-ray studies were conducted by using a Rigaku Ultima IV diffractometer. Thermogravimetric analysis (TGA) was carried out using a TA Shimadzu instrument. FESEM experiments were performed on a JEOL instrument; each sample was well dispersed in methanol, drop cast on a silicon wafer, dried and coated with gold using a working distance of 15–22 mm and a voltage of 3–5 kV. High-resolution transmission electron microscopy (HRTEM) was performed on a JEOL JEM-F-200 microscope. For sample preparation, 1 mg of the material was dispersed in 10 mL of methanol and sonicated for 15 min to obtain a homogeneous suspension. A drop of the suspension was then deposited onto a copper grid and allowed to dry under ambient conditions prior to analysis.

Single crystal X-ray data collection and refinements. For **2**-**4**, suitable single crystals were chosen and mounted on the goniometer head using a nylon loop of appropriate dimension and mineral oil. Initial crystal evaluation and data collection were performed at room temperature using a fully automated Kappa APEX II diffractometer equipped with a CCD detector and sealed-tube monochromated Mo Kα radiation through APEX2.[S1] The program SAINT[S1] was used to integrate the data, fitting reflection profiles, and obtaining values of F^2 and $\sigma(F^2)$ for each reflection. Data were also corrected for Lorentz and polarization effects. The subroutine XPREP[S1] was used for the processing of data that included determination of space group, application of an absorption correction (SADABS[S1]), merging of data, and generation of files necessary for solution and refinement. The crystal structures were solved by direct methods using the SHELXS program of the SHELXT[S2] package and refined using full-matrix least-squares methods with SHELXL-2014. Several full-matrix least-squares/difference Fourier cycles were performed, locating the remainder of the nonhydrogen atoms. In order to improve the R-factors and to address the residual electron density for any disordered solvent molecules, certain reflections with strong disagreement between Fo and Fc were omitted and/or the solvent masking option in Olex2 software[S3] was applied, whenever appropriate and necessary (for **3** and **4**). Hydrogen atoms except for those of lattice water molecule(s) for all structures were added at the calculated positions. All figures were drawn using OLEX2,[S3] Mercury V 3.10.2,[S4] and DIAMOND V 3.2.[S5]

Density functional theory (DFT) calculation. Using the Gaussian 09 suite of packages, calculations were performed. For the optimization of the structure, hybrid functional, Becke's three-parameter exchange, and the Lee−Yang−Parr correlation functional (B3LYP) at a split valence basis set 6-31G(d,p) were used.[S6]

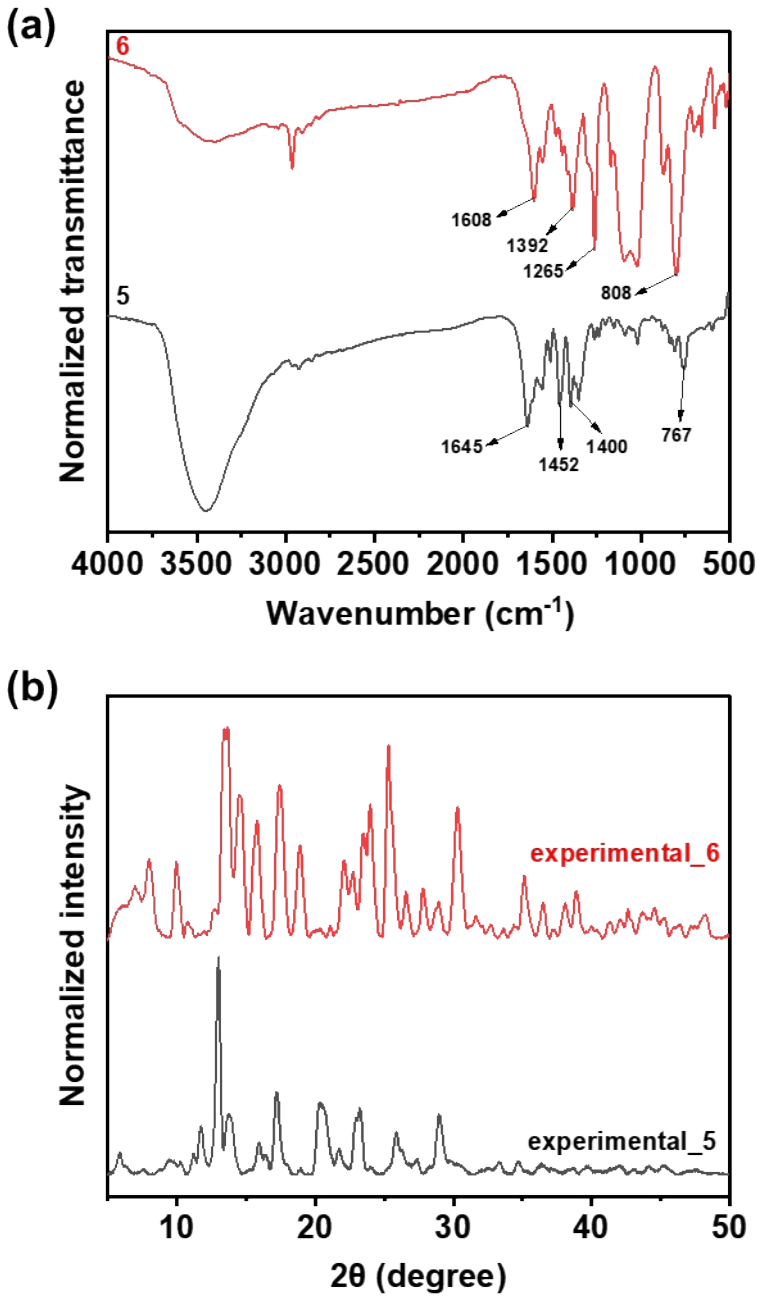

Fig. S1 FTIR spectra and PXRD patterns of **5** and **6**. These spectra and diffractograms match exactly with the ones reported earlier in References.

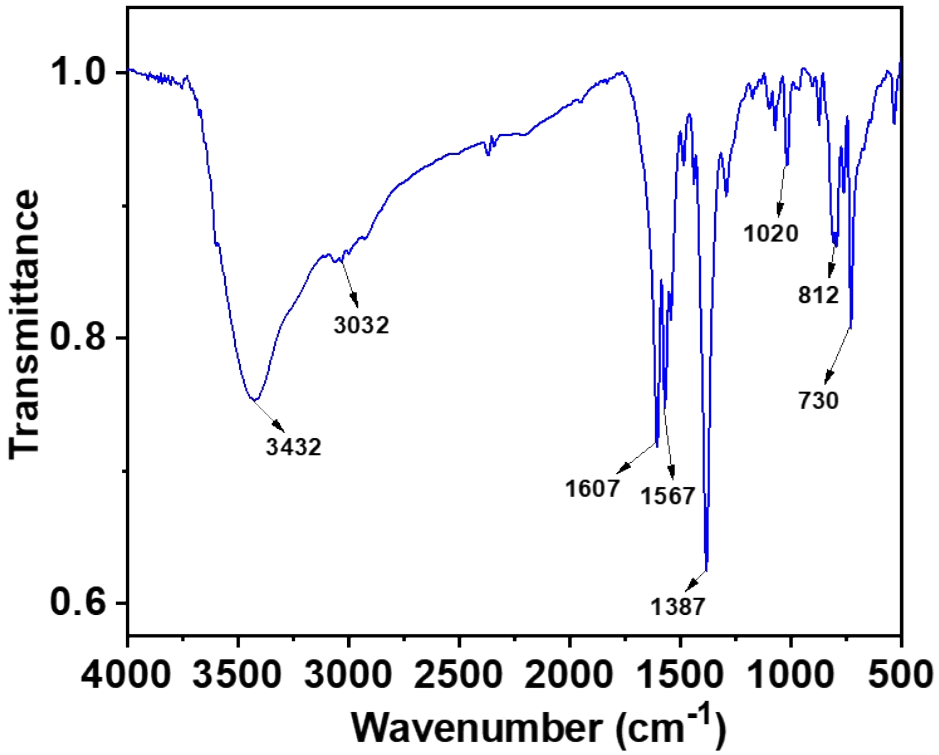

Fig. S2 FTIR spectrum of **1**.

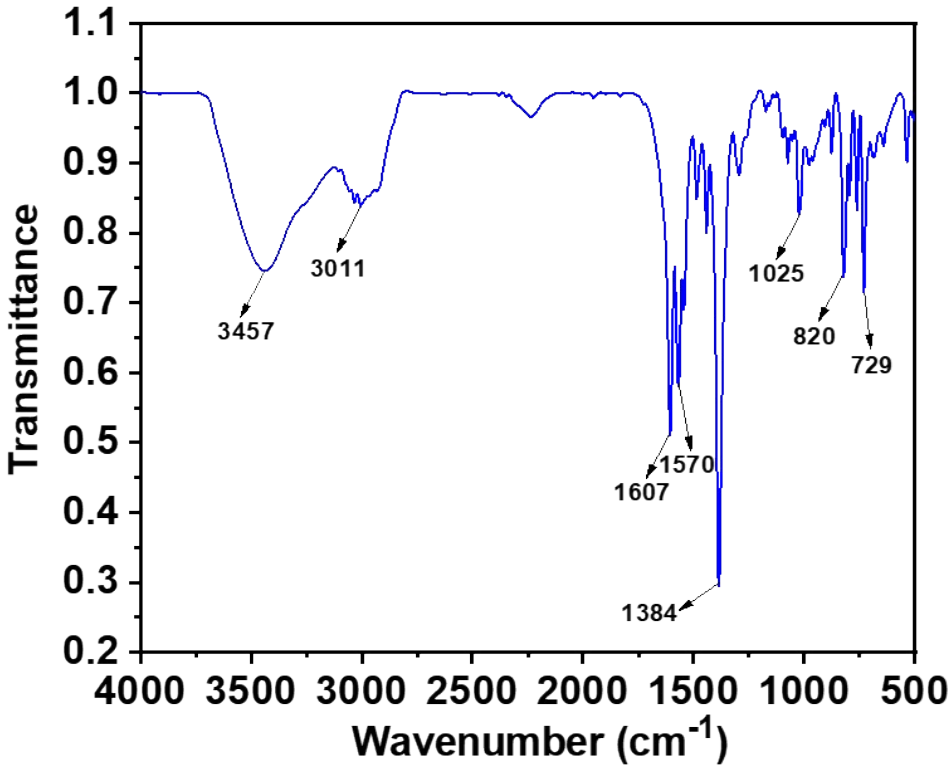

Fig. S3 FTIR spectrum of **2**.

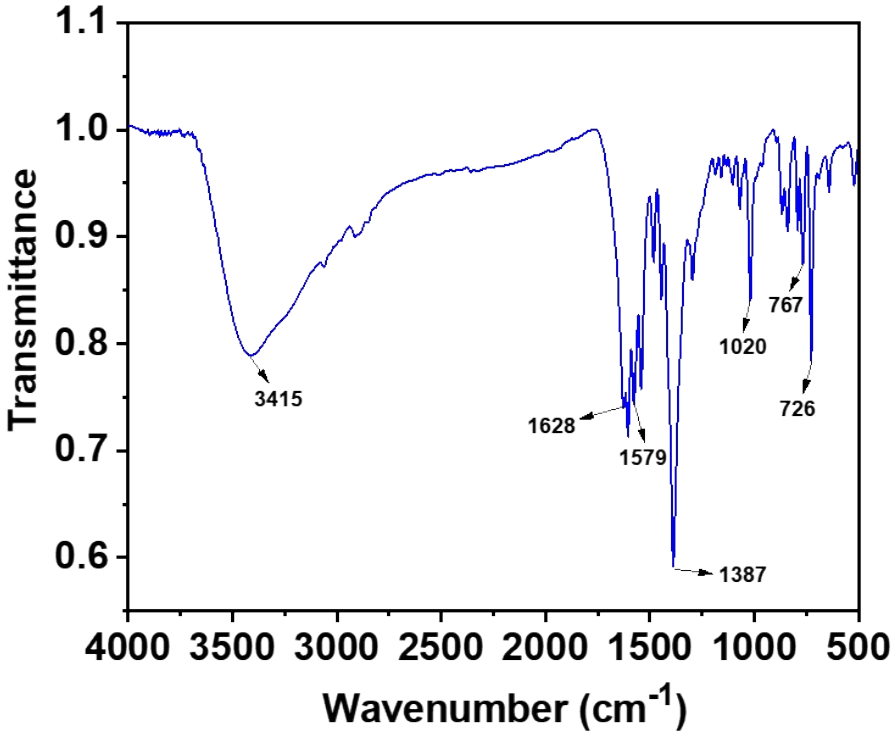

Fig. S4 FTIR spectrum of **3**.

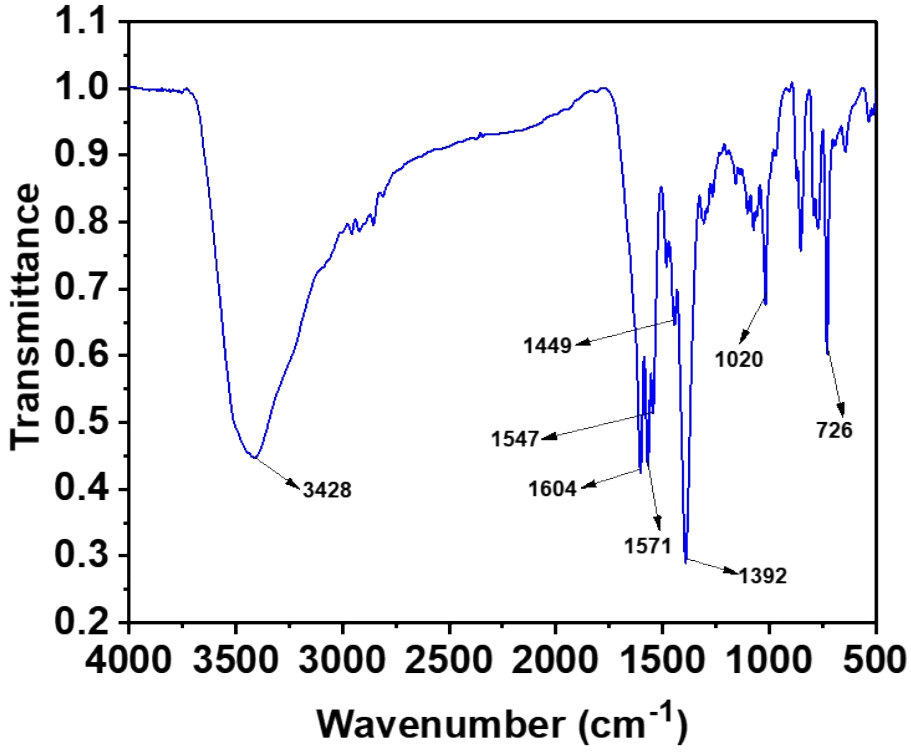

Fig. S5 FTIR spectrum of **4**.

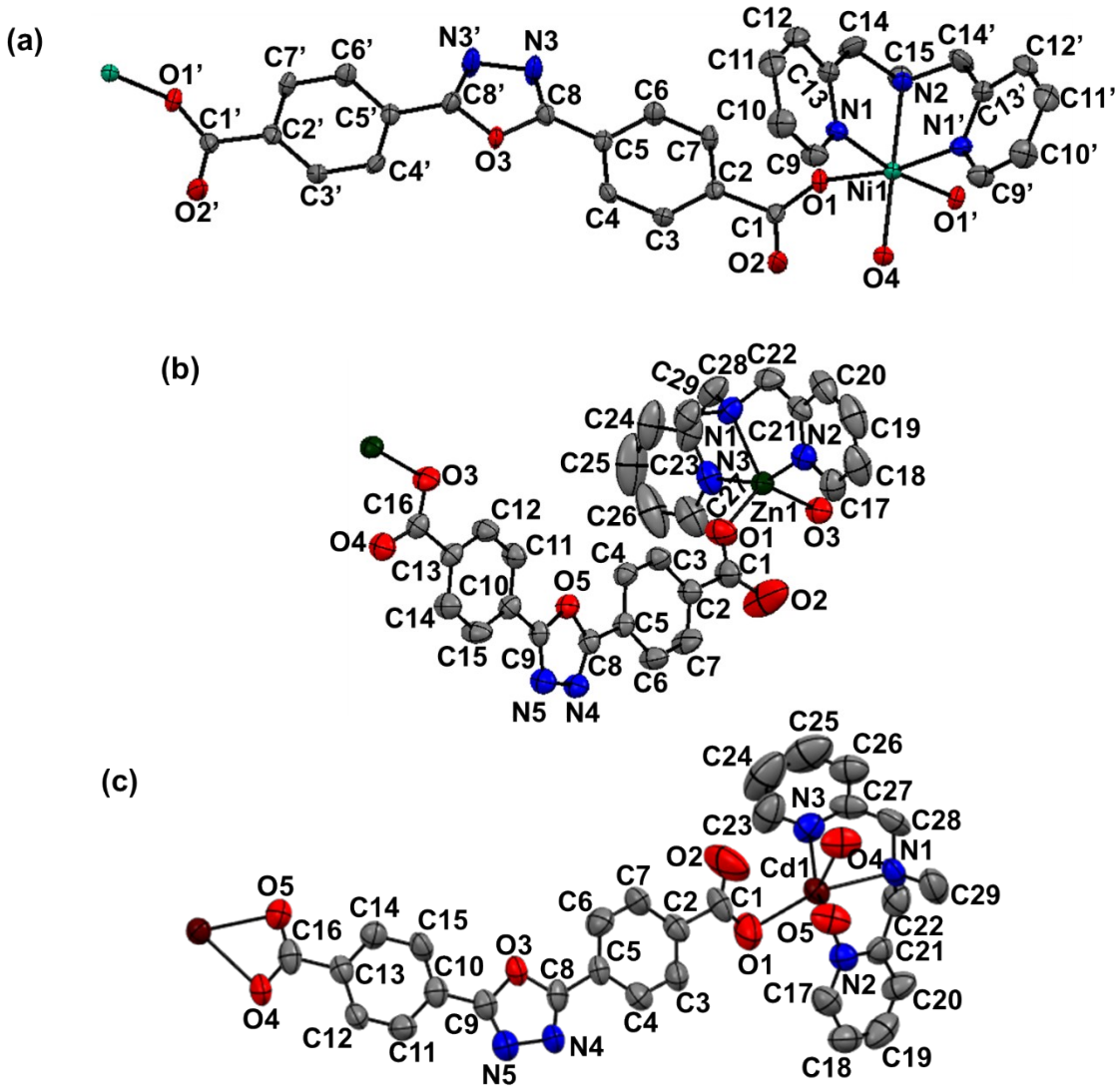

Fig. S6 (a-c) Fully labelled view of the repeat units of the polymeric structures, **2-4**, respectively. Non-hydrogen atoms are depicted as ellipsoids with 50% probability. Hydrogen atoms are not shown for clarity.

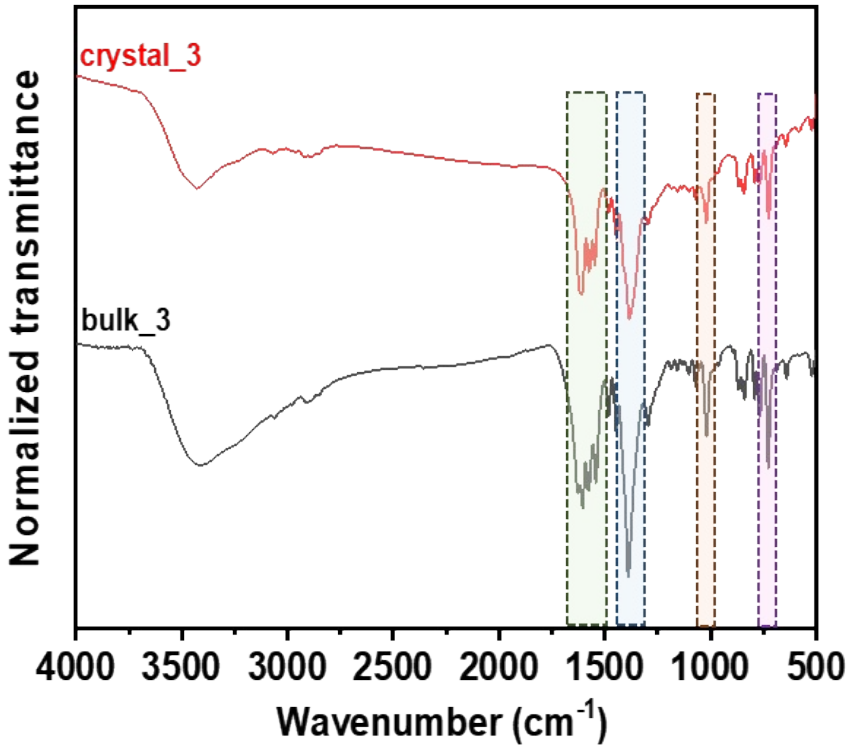

Fig. S7 FTIR spectra of as-synthesized **3** and its crystals.

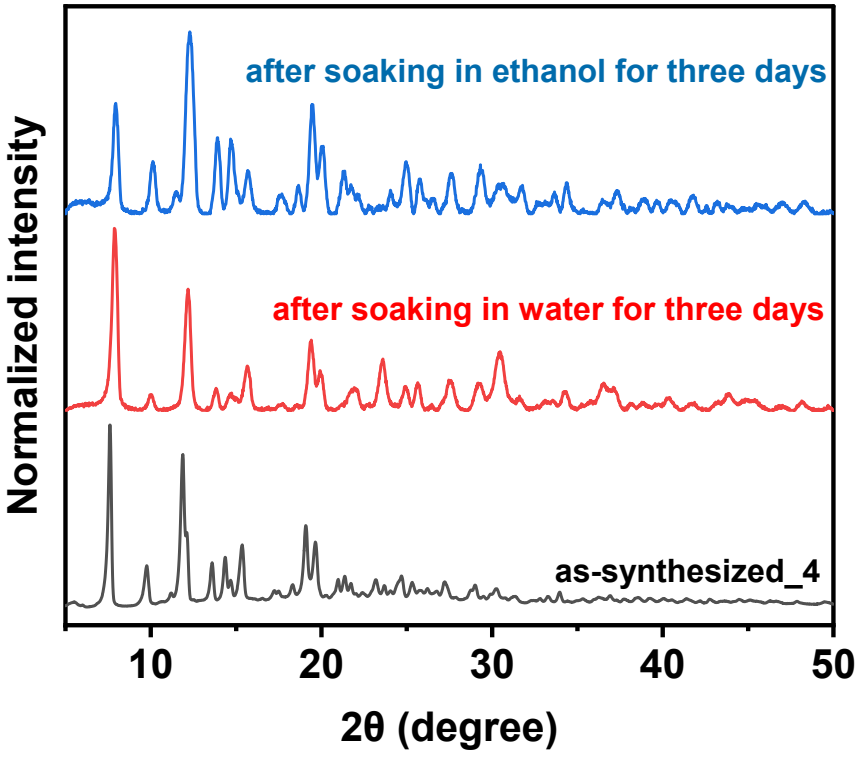

Fig. S8 Stability of **4** in water and ethanol.

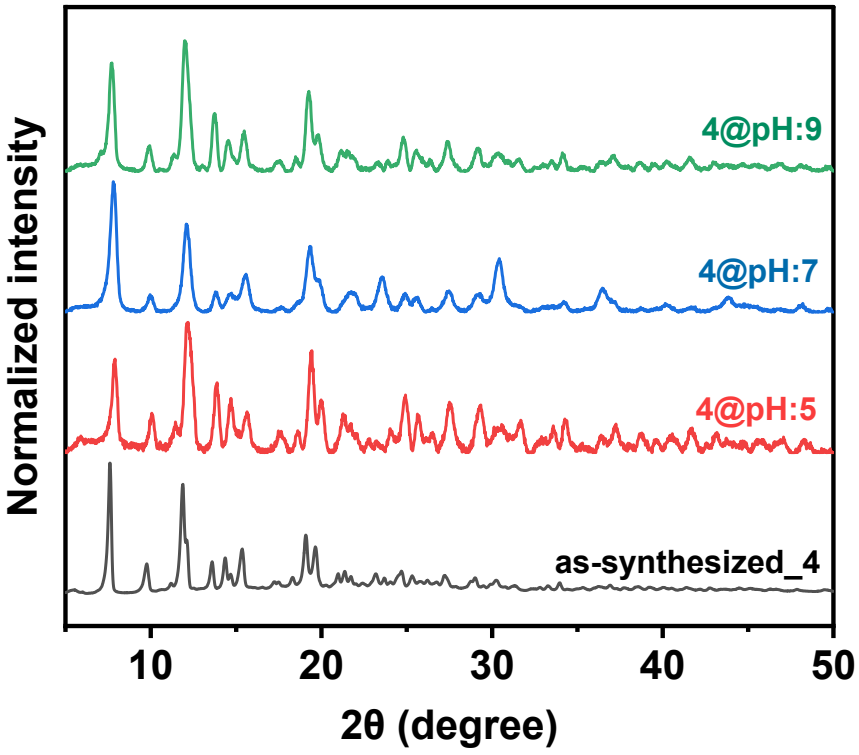

Fig. S9 Stability of **4** under different pH conditions.

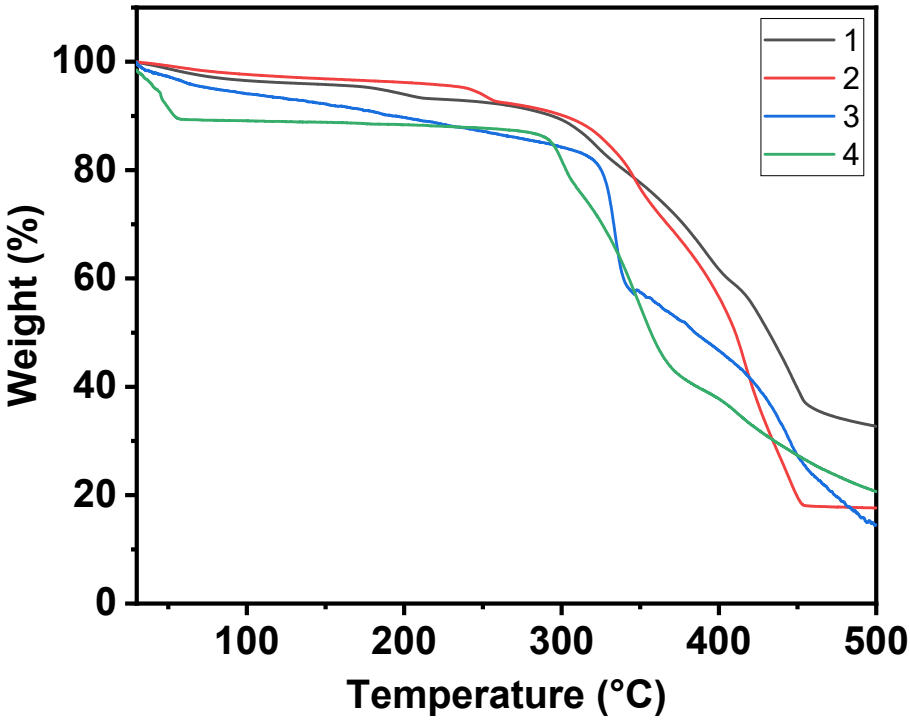

Fig. S10 TG profiles of **1-4**.

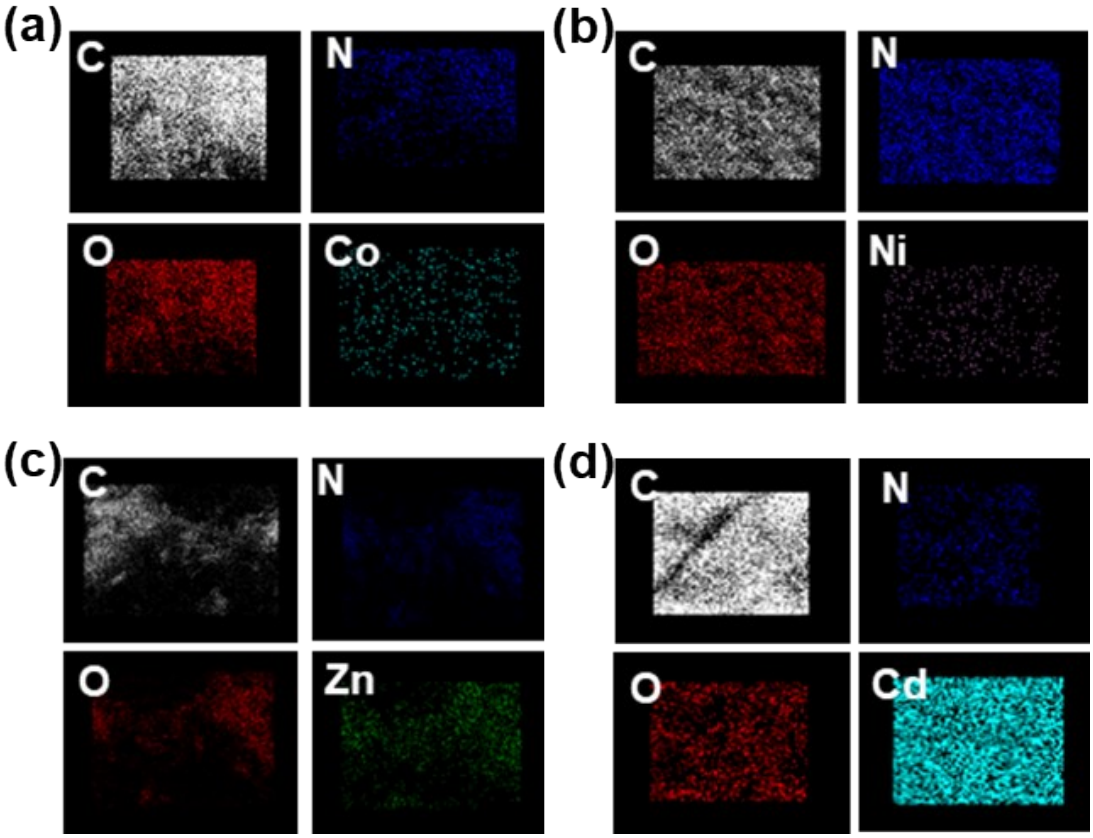

Fig. S11 (a-d) Elemental mapping highlighting the homogeneous distribution of the component elements in **1**-**4**, respectively.

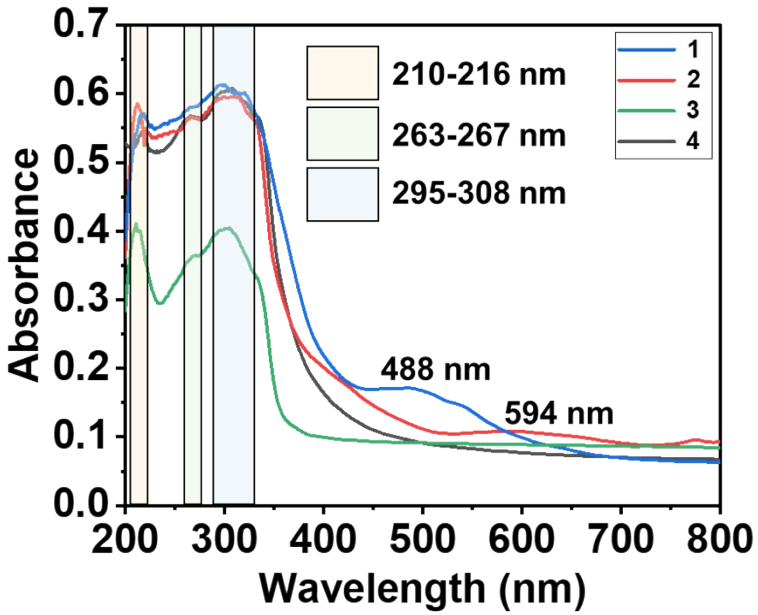

Fig. S12 Solid-state diffuse reflectance spectra of **1**-**4**.

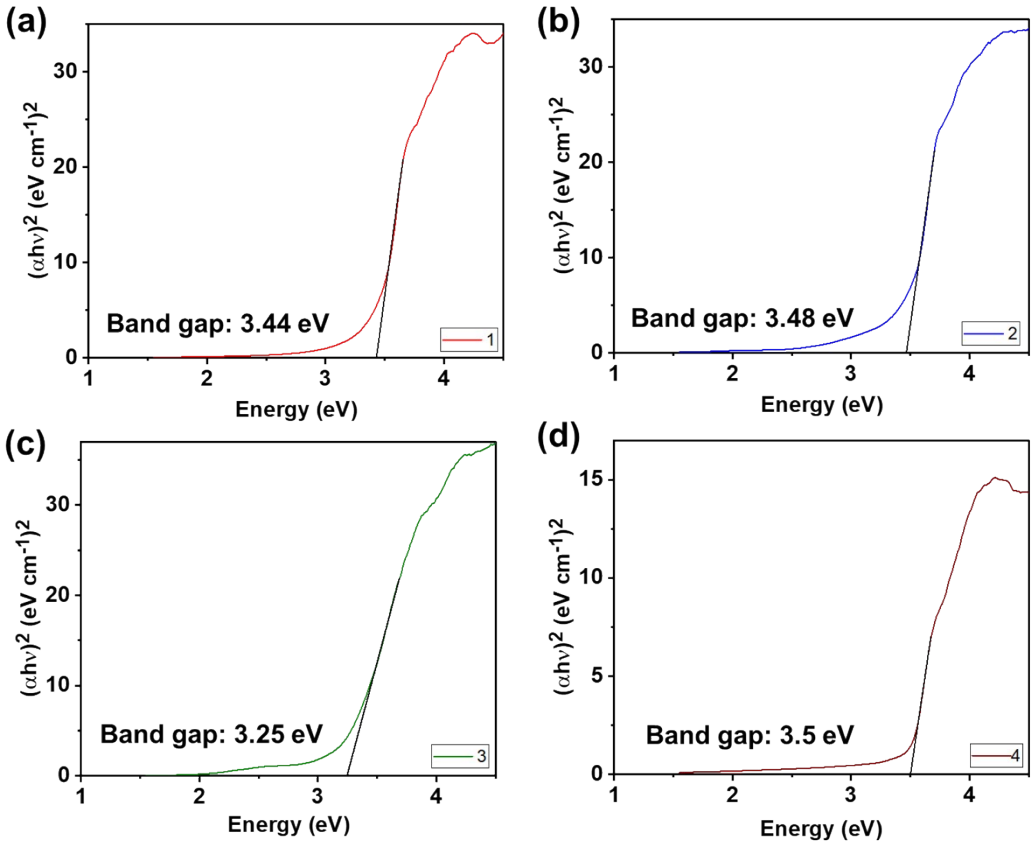

Fig. S13 (a-d) Tauc plot and band gap energy value for **1-4**, respectively.

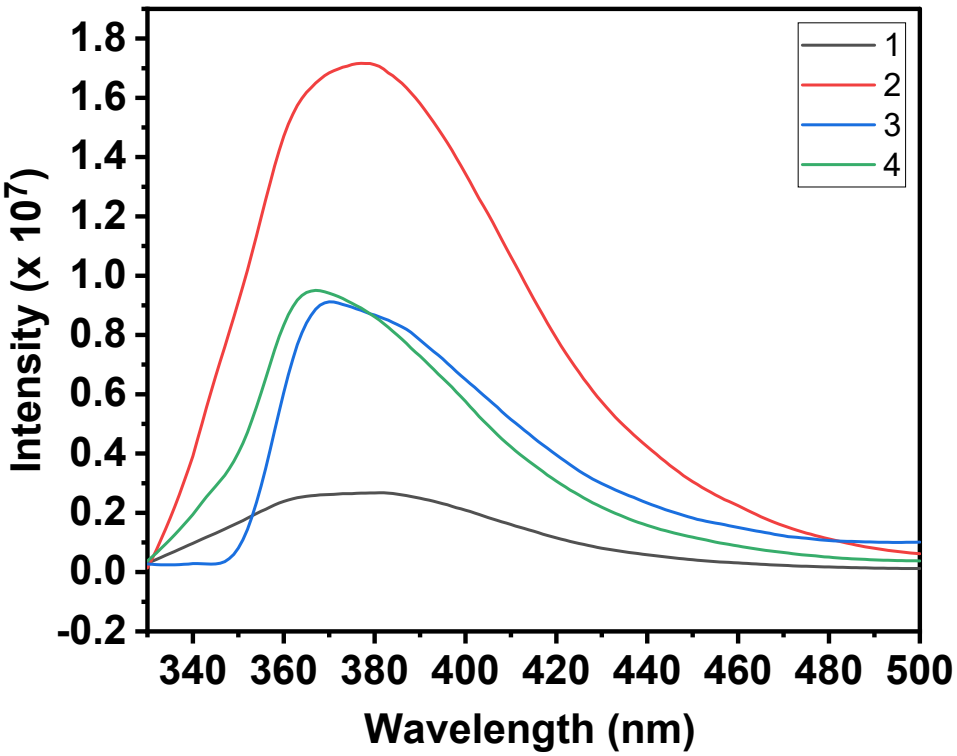

Fig. S14 Emission spectra of homogeneous suspensions of **1-4** in water.

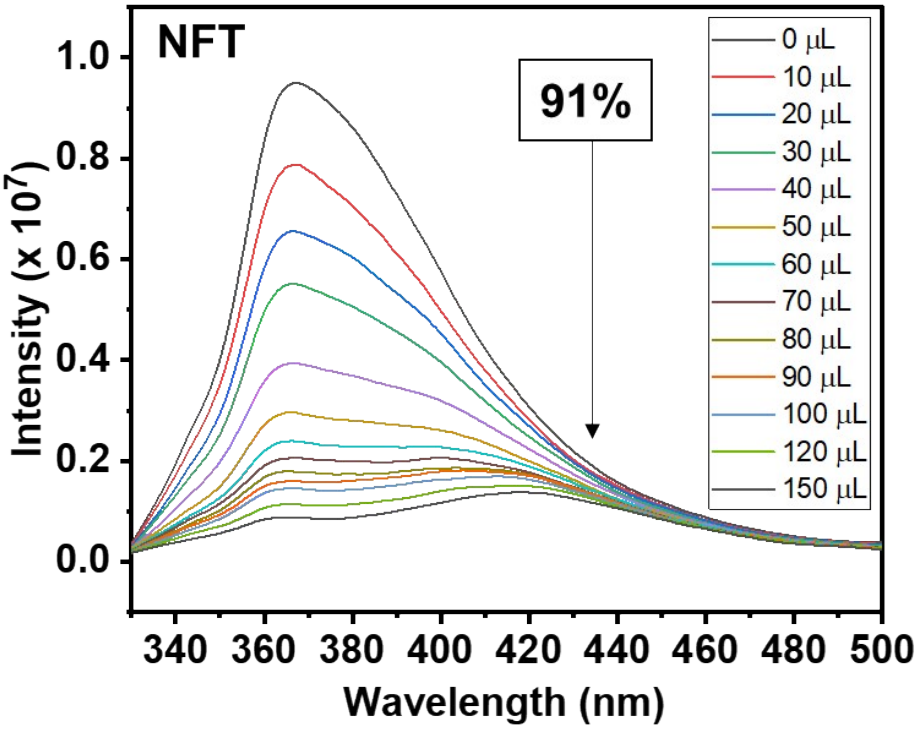

Fig. S15 Emission spectra of **4** dispersed in aqueous solution upon incremental addition of NFT solution (1 mM).

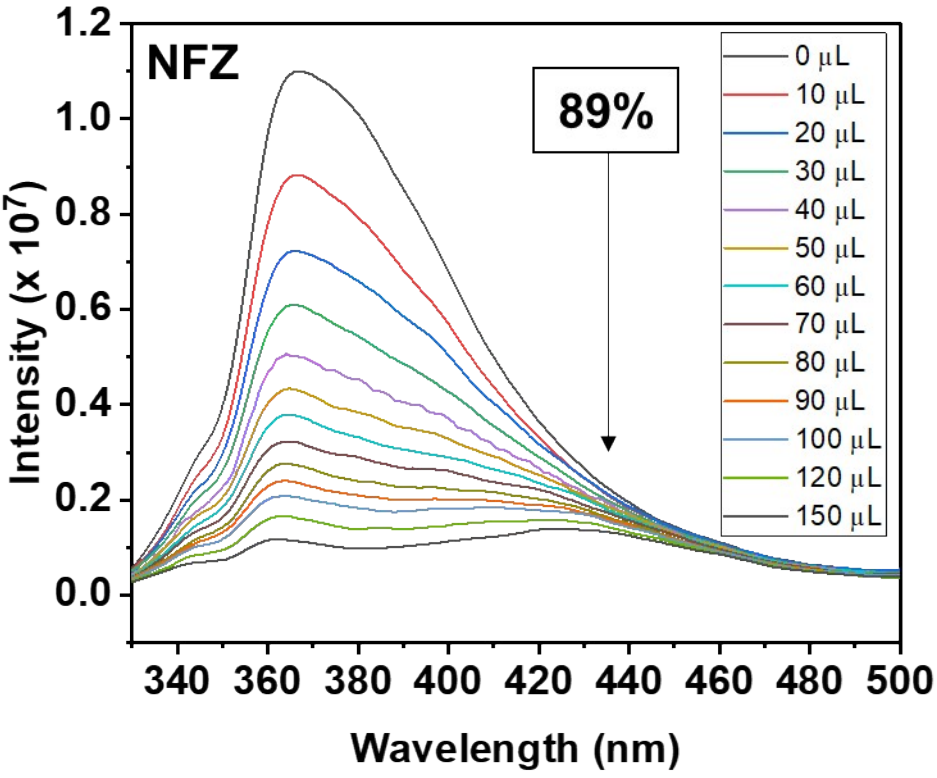

Fig. S16 Emission spectra of **4** dispersed in aqueous solution upon incremental addition of NFZ solution (1 mM).

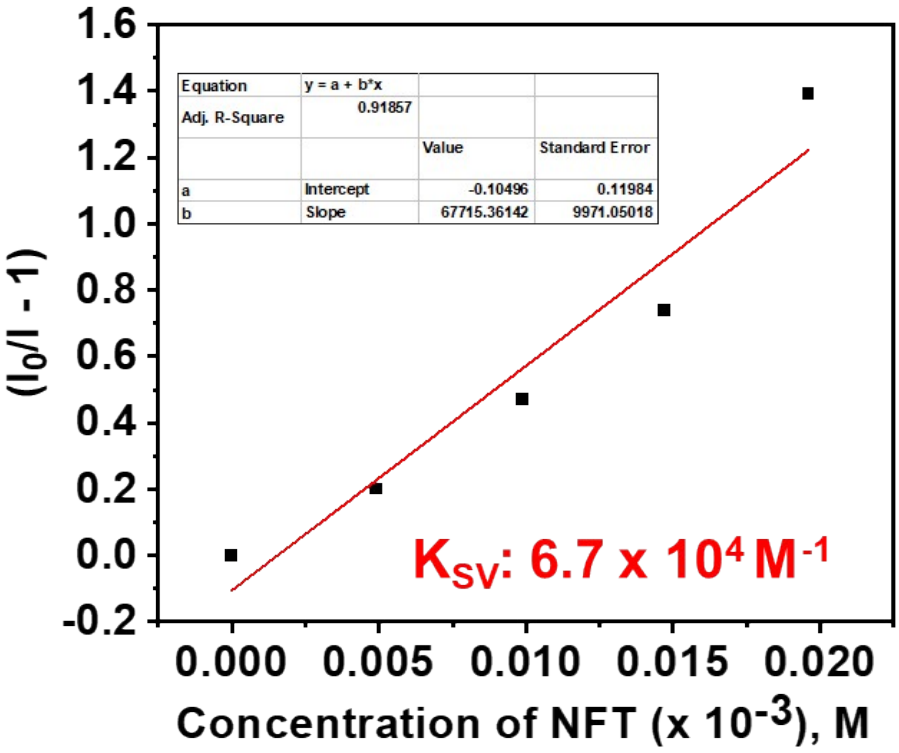

Fig. S17 Stern-Volmer (SV) plot for NFT of **4**. The relative fluorescence intensity is linear with NFT concentration in the range of 0-20 µM, $I_0/I = 1 + 67715.36$ ([NFT]) ($R^2 = 0.91857$).

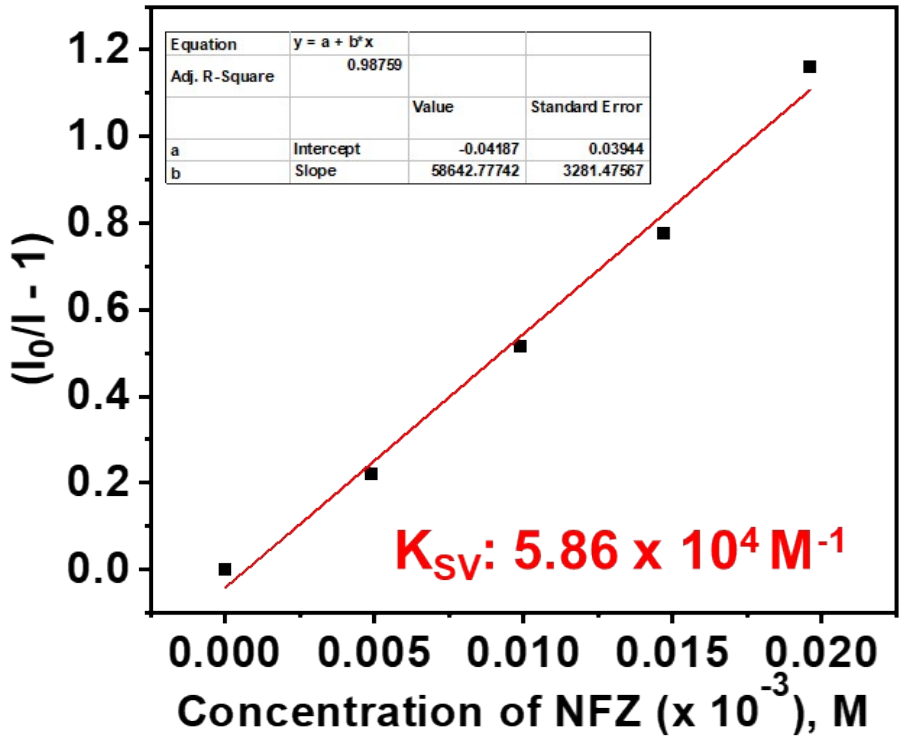

Fig. S18 Stern-Volmer (SV) plot for NFZ of **4**. The relative fluorescence intensity is linear with NFZ concentration in the range of 0-20 µM, $I_0/I = 1 + 58642.77$ ([NFZ]) ($R^2 = 0.98759$).

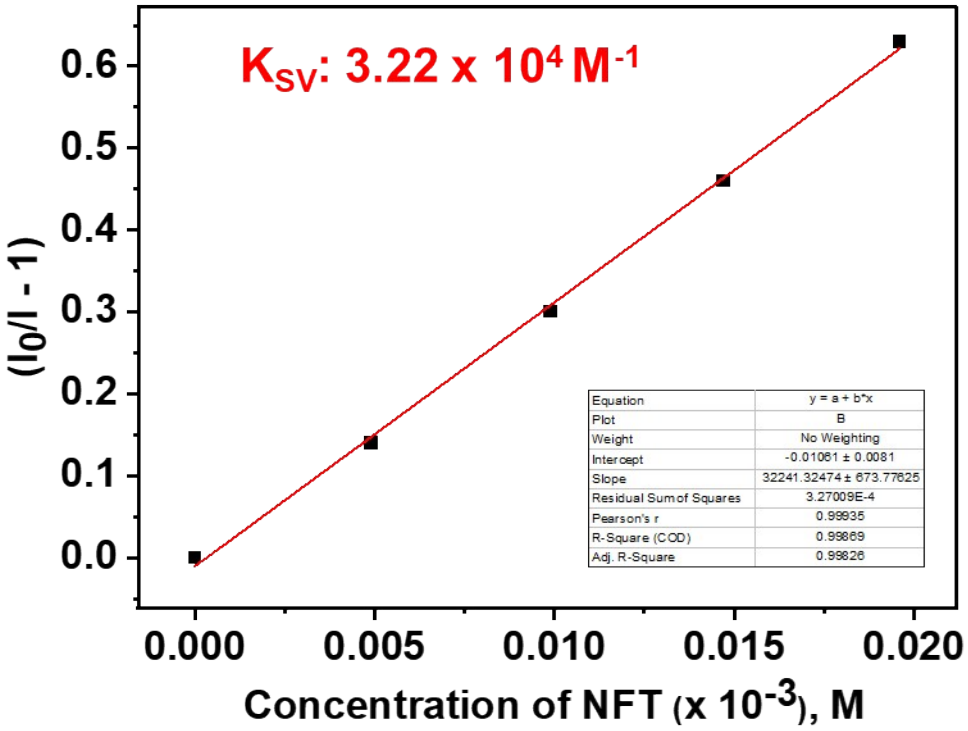

Fig. S19 Stern-Volmer (SV) plot for NFT of **1**. The relative fluorescence intensity is linear with NFT concentration in the range of 0-20 µM, $I_0/I = 1 + 32241.32$ ([NFT]) ($R^2 = 0.99826$).

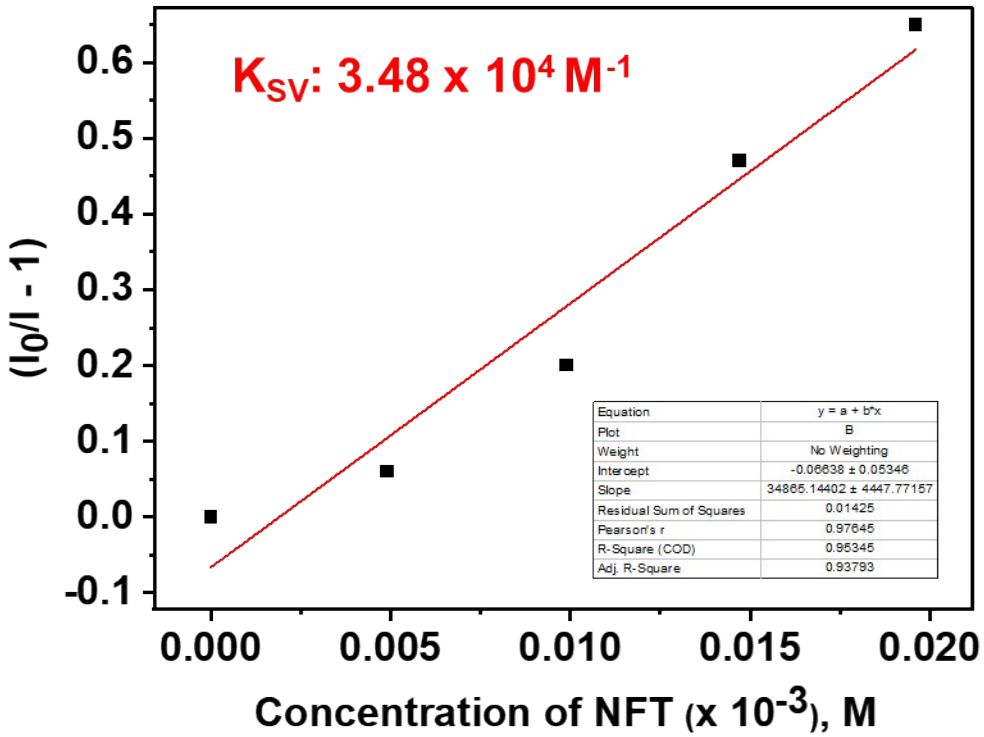

Fig. S20 Stern-Volmer (SV) plot for NFT of **2**. The relative fluorescence intensity is linear with NFT concentration in the range of 0-20 µM, $I_0/I = 1 + 34865.144$ ([NFT]) ($R^2 = 0.93793$).

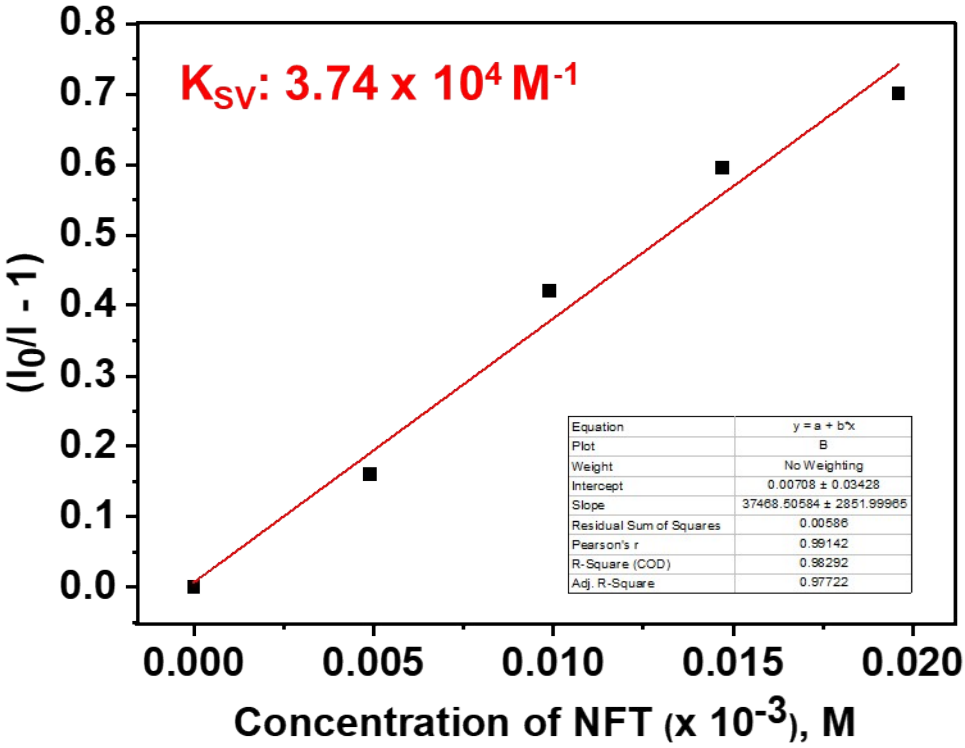

Fig. S21 Stern-Volmer (SV) plot for NFT of **3**. The relative fluorescence intensity is linear with NFT concentration in the range of 0-20 μM, $I_0/I = 1 + 37468.5$ ([NFT]) ($R^2 = 0.97722$).

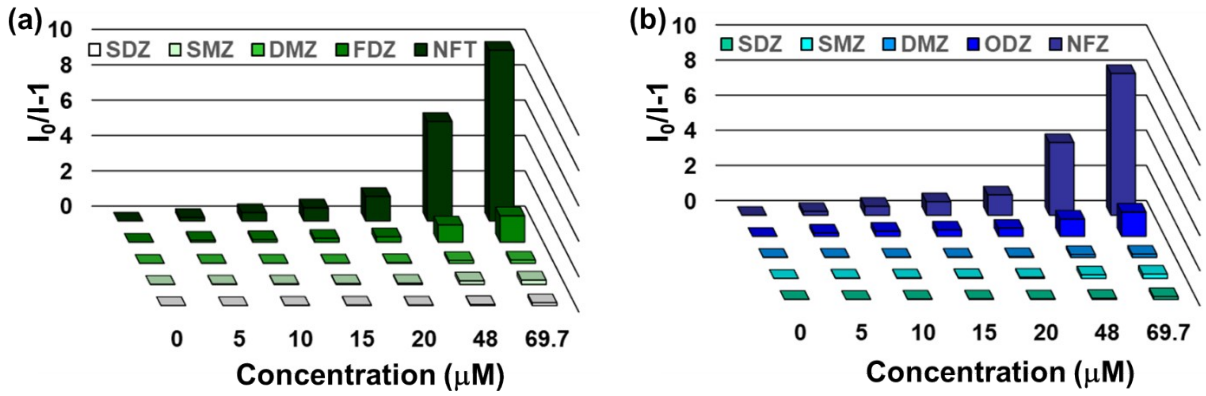

Fig. S22 3D Stern–Volmer plot of **1** dispersed in water in presence of different antibiotics.

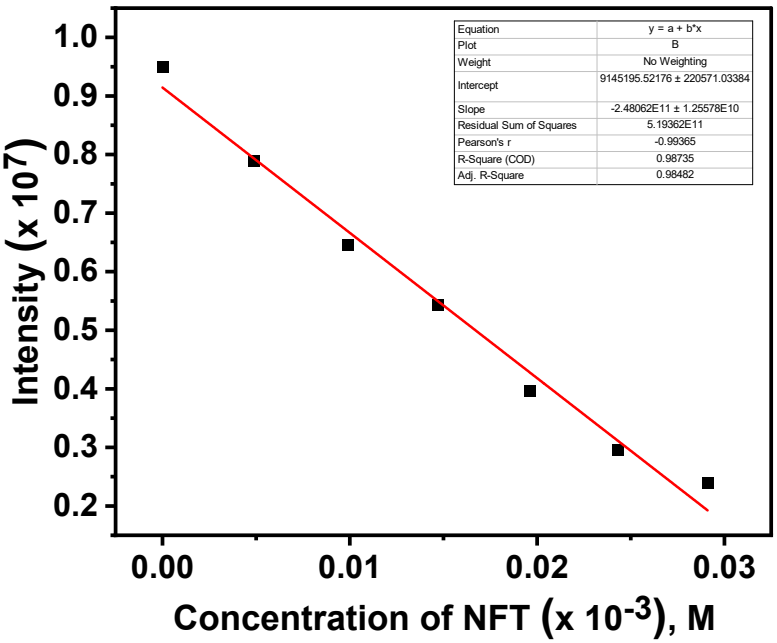

Fig. S23 Linear region of fluorescence intensity of **4** upon incremental addition of NFT (1 mM stock solution) at λ_{em}= 362 nm (upon λ_{exc} = 310 nm) (R^2 = 0.98482).

Calculation of Standard Deviation of 4:

Blank Readings	**Fl Intensity**
Reading 1	9.64 x 10^6
Reading 2	9.53 x 10^6
Reading 3	9.51 x 10^6
Reading 4	9.46 x 10^6
Reading 5	9.49 x 10^6
Standard Deviation (σ)	6.8775 x 10^4

Determination of Detection Limit of 4 in presence of NFT:

Detection limit was calculated using the following equation:

Detection limit = 3σ/m

Where 'σ' is the calculated standard deviation from five blank measurements and 'm' is the slope obtained from the plot of fluorescence emission with increasing concentration of NFT.

Detection Limit: 197 ppb or 0.831 μmol/L

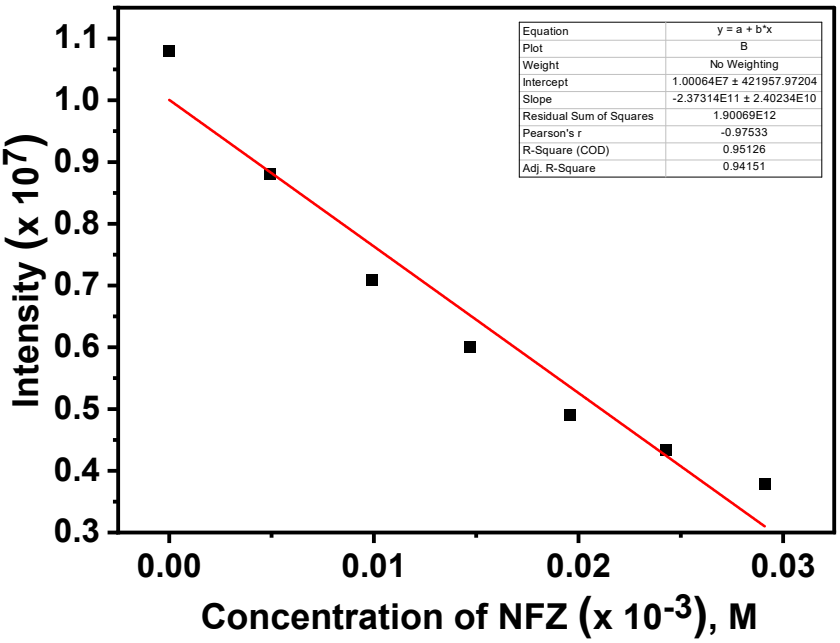

Fig. S24 Linear region of fluorescence intensity of **4** upon incremental addition of NFZ (1 mM stock solution) at λ_{em}= 362 nm (upon λ_{exc} = 310 nm) (R^2 = 0.94151).

Calculation of Standard Deviation of **4**:

Blank Readings	**Fl Intensity**
Reading 1	9.64 x 10^6
Reading 2	9.53 x 10^6
Reading 3	9.51 x 10^6
Reading 4	9.46 x 10^6
Reading 5	9.49 x 10^6
Standard Deviation (σ)	6.8775 x 10^4

Determination of Detection Limit of 4 in presence of NFZ:

Detection limit was calculated using the following equation:

Detection limit = 3σ/m

Where 'σ' is the calculated standard deviation from five blank measurements and 'm' is the slope obtained from the plot of fluorescence emission with increasing concentration of NFZ.

Detection Limit: 172 ppb or 0.869 μmol/L

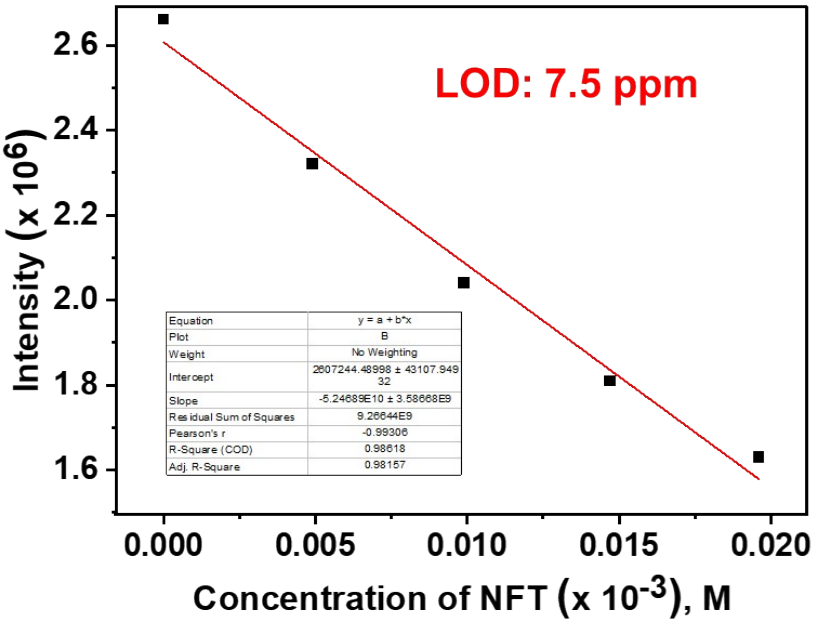

Fig. S25 Linear region of fluorescence intensity of **1** upon incremental addition of NFT (1 mM stock solution) at λ_{em}= 380 nm (upon λ_{exc} = 310 nm) (R^2 = 0.98157).

Calculation of Standard Deviation of 1:

Blank Readings	**Fl Intensity**
Reading 1	1.9 x 10^6
Reading 2	2.01 x 10^6
Reading 3	3.11 x 10^6
Reading 4	2.99 x 10^6
Reading 5	2.66 x 10^6
Standard Deviation (σ)	5.55 x 10^5

Determination of Detection Limit of 1 in presence of NFT:

Detection limit was calculated using the following equation:

Detection limit = 3σ/m

Where 'σ' is the calculated standard deviation from five blank measurements and 'm' is the slope obtained from the plot of fluorescence emission with increasing concentration of NFT.

Detection Limit: 7.5 ppm or 31.7 μmol/L

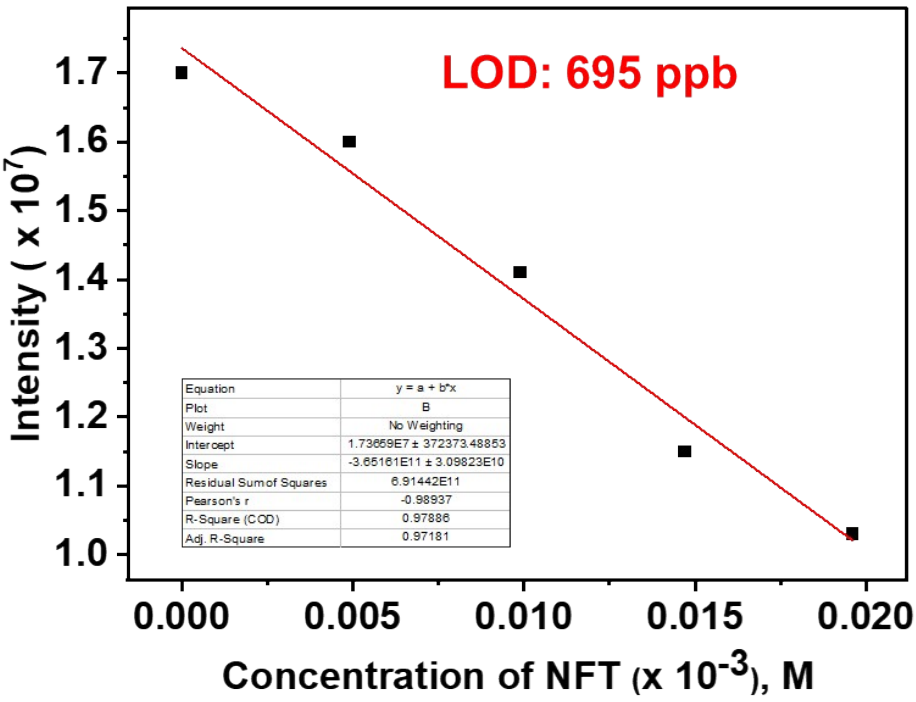

Fig. S26 Linear region of fluorescence intensity of **2** upon incremental addition of NFT (1 mM stock solution) at λ_{em}= 377 nm (upon λ_{exc} = 310 nm) (R^2 = 0.97181).

Calculation of Standard Deviation of 2:

Blank Readings	**Fl Intensity**
Reading 1	1.79 x 10^7
Reading 2	1.7 x 10^7
Reading 3	1.72 x 10^7
Reading 4	1.71 x 10^7
Reading 5	1.72 x 10^7
Standard Deviation (σ)	3.56 x 10^5

Determination of Detection Limit of 2 in presence of NFT:

Detection limit was calculated using the following equation:

Detection limit = 3σ/m

Where 'σ' is the calculated standard deviation from five blank measurements and 'm' is the slope obtained from the plot of fluorescence emission with increasing concentration of NFT.

Detection Limit: 695 ppb or 2.92 μmol/L

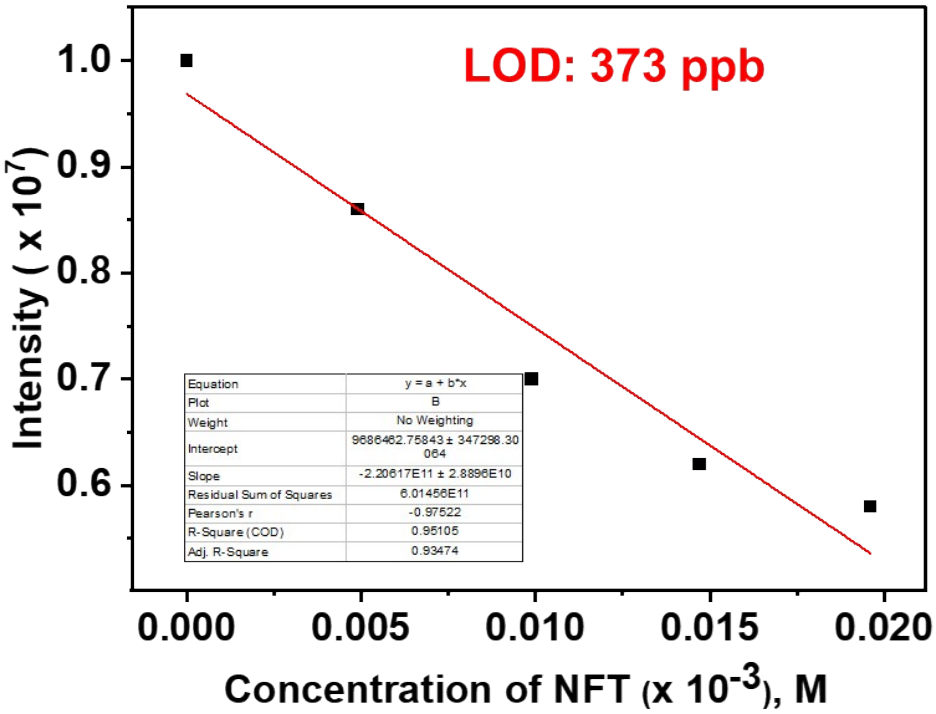

Fig. S27 Linear region of fluorescence intensity of **3** upon incremental addition of NFT (1 mM stock solution) at λ_{em}= 370 nm (upon λ_{exc} = 310 nm) (R^2 = 0.93474).

Calculation of Standard Deviation of 3:

Blank Readings	**Fl Intensity**
Reading 1	1.00 x 10^7
Reading 2	0.98 x 10^7
Reading 3	0.97 x 10^7
Reading 4	0.99 x 10^7
Reading 5	0.99 x 10^7
Standard Deviation (σ)	1.16 x 10^5

Determination of Detection Limit of 3 in presence of NFT:

Detection limit was calculated using the following equation:

Detection limit = 3σ/m

Where 'σ' is the calculated standard deviation from five blank measurements and 'm' is the slope obtained from the plot of fluorescence emission with increasing concentration of NFT.

Detection Limit: 373 ppb or 1.57 μmol/L

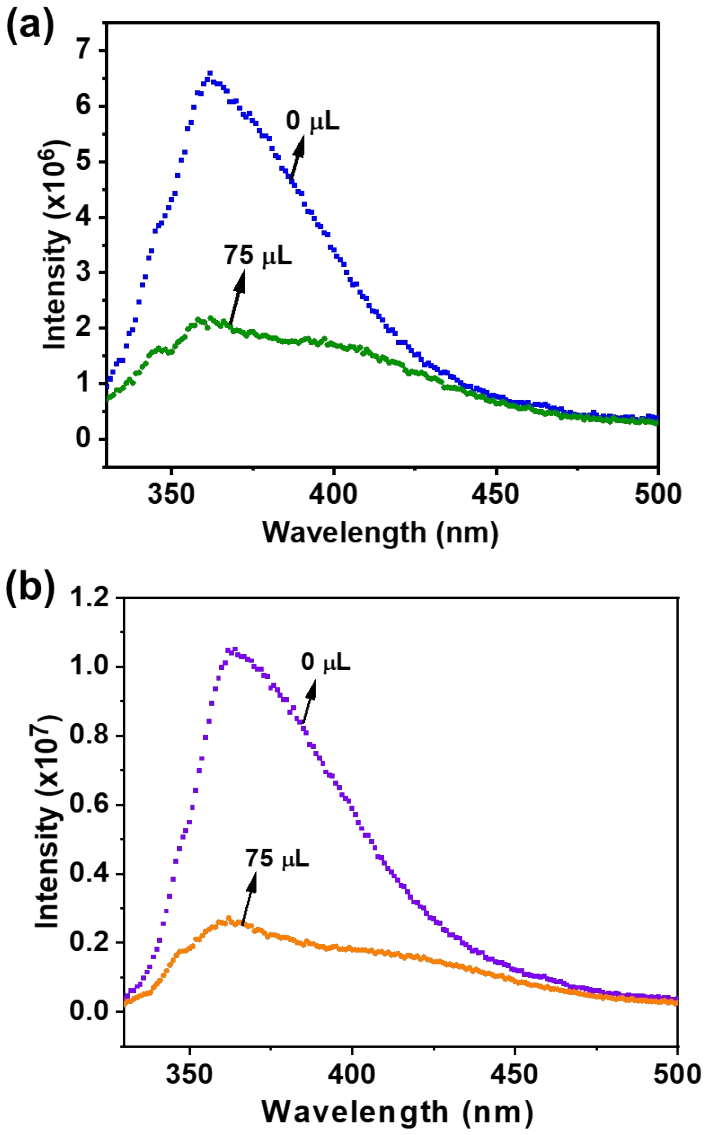

Fig. S28 Emission spectra of **4** before (0 s) and after (20 s) addition of 75 μL of NFT (a) and NFZ (b).

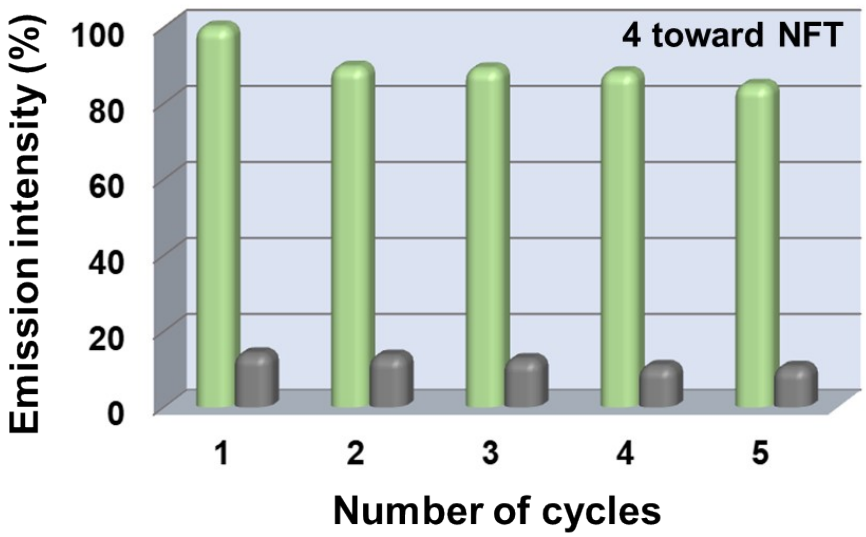

Fig. S29 Recyclability tests for **4** in presence of NFT.

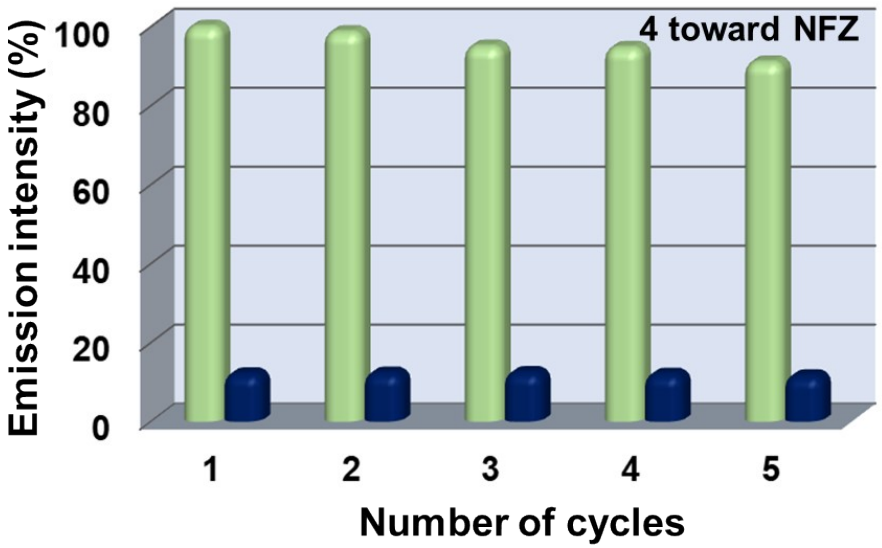

Fig. S30 Recyclability tests for **4** in presence of NFZ.

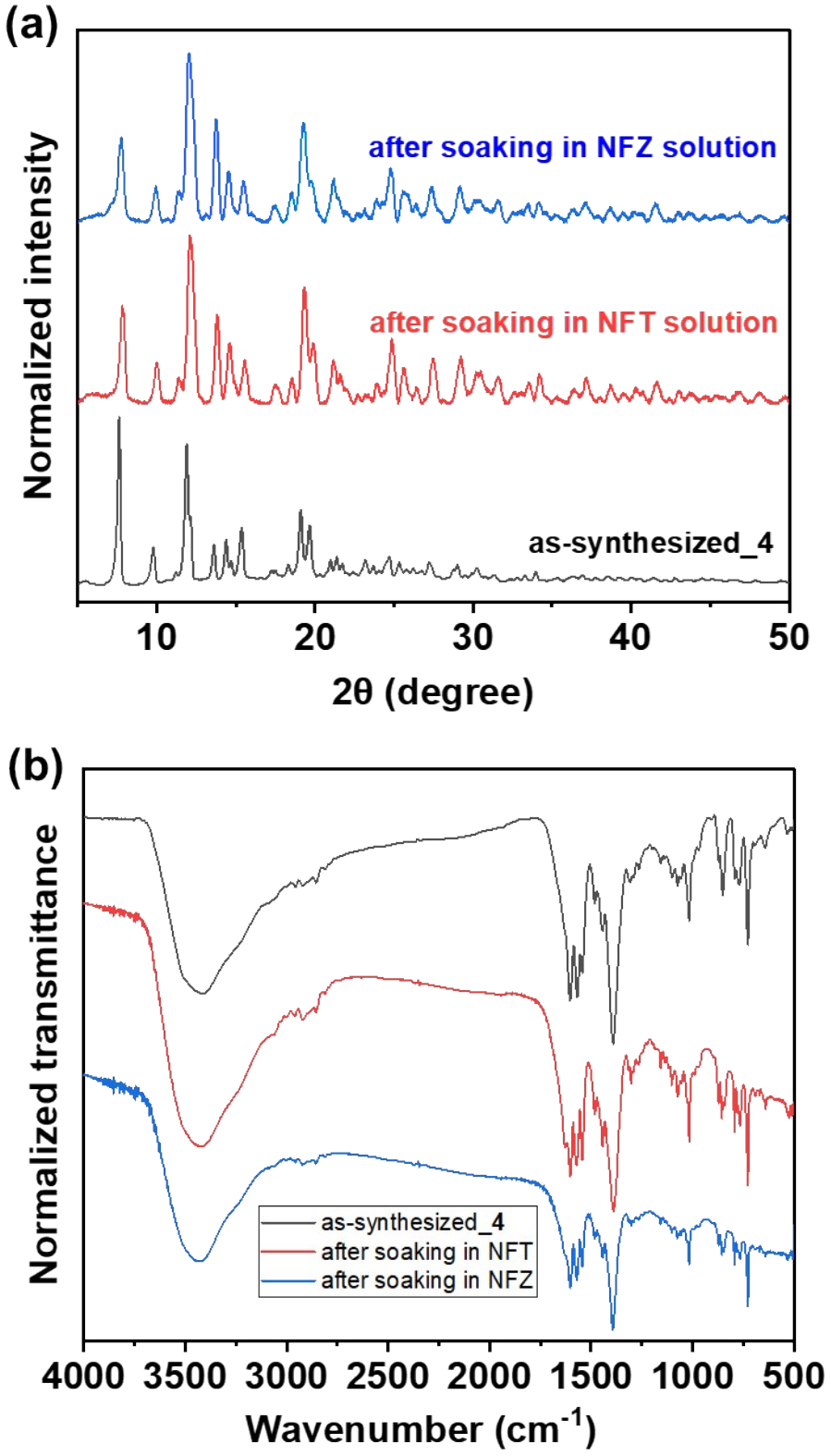

Fig. S31 (a-b) Stability of **4** before and after soaking in NFT and NFZ solutions for 24 h.

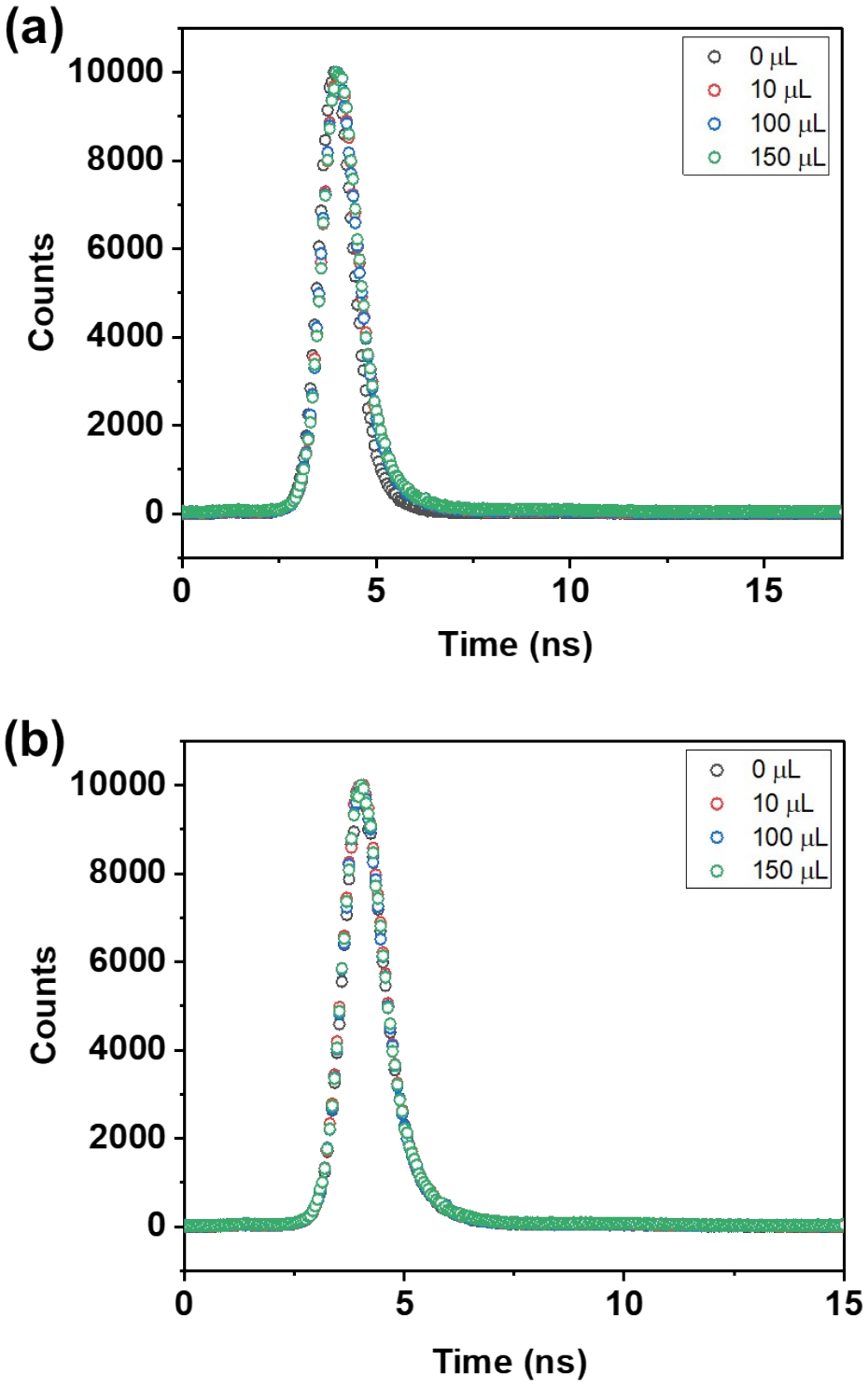

Fig. S32 Lifetime decay curves of **4** before and after the addition of NFT (a) and NFZ (b) in aqueous media.

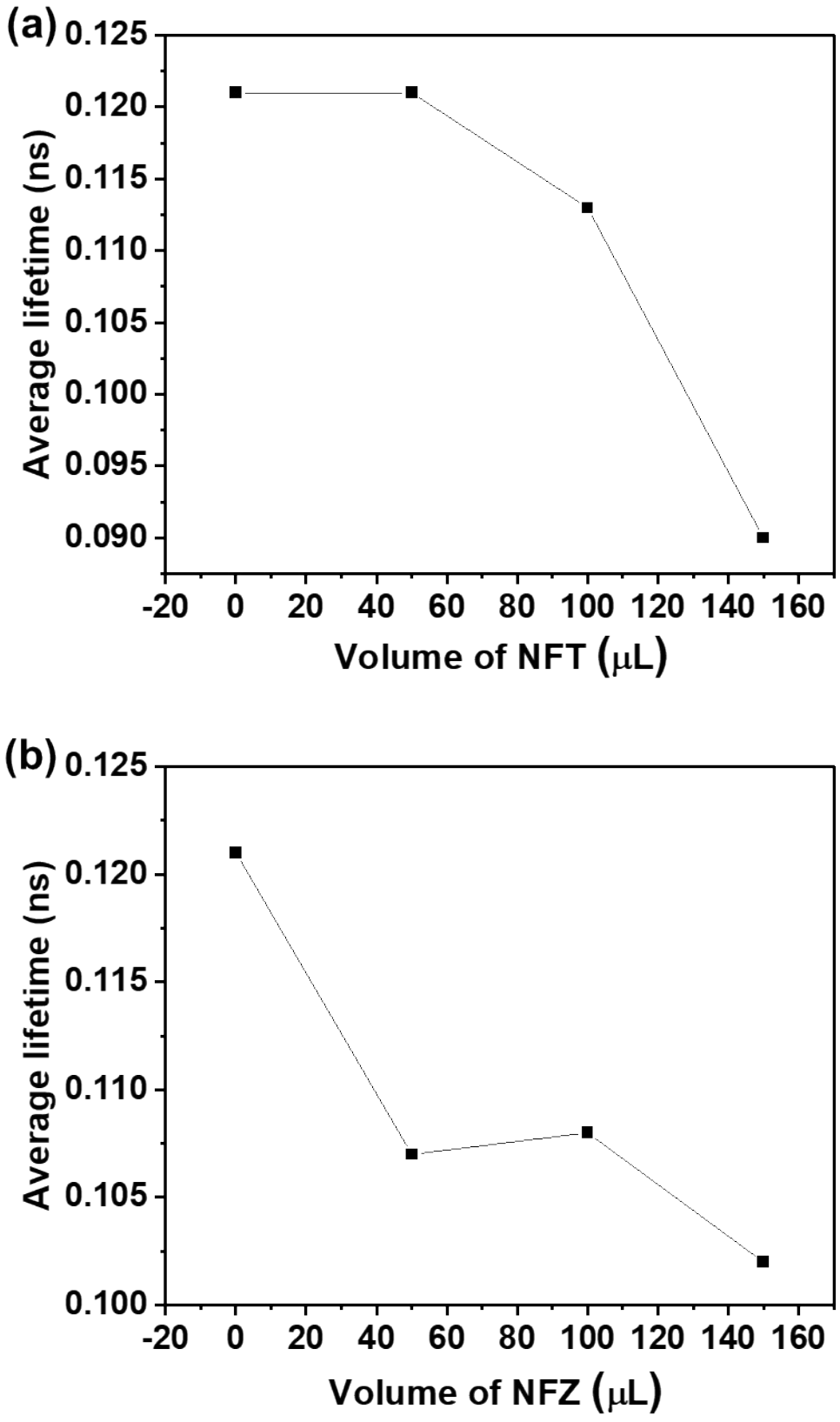

Fig. S33 (a-b) Plot of average lifetime vs volume of NFT and NFZ, respectively.

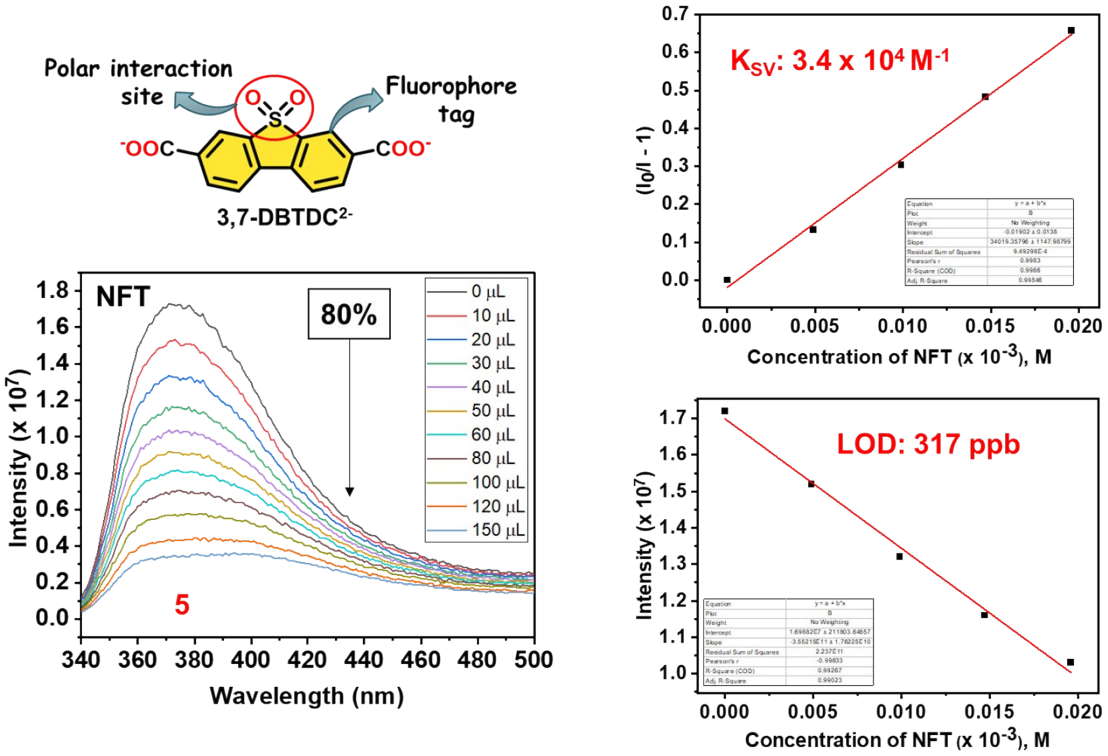

Fig. S34 Fluorescence based detection of NFT by **5**.

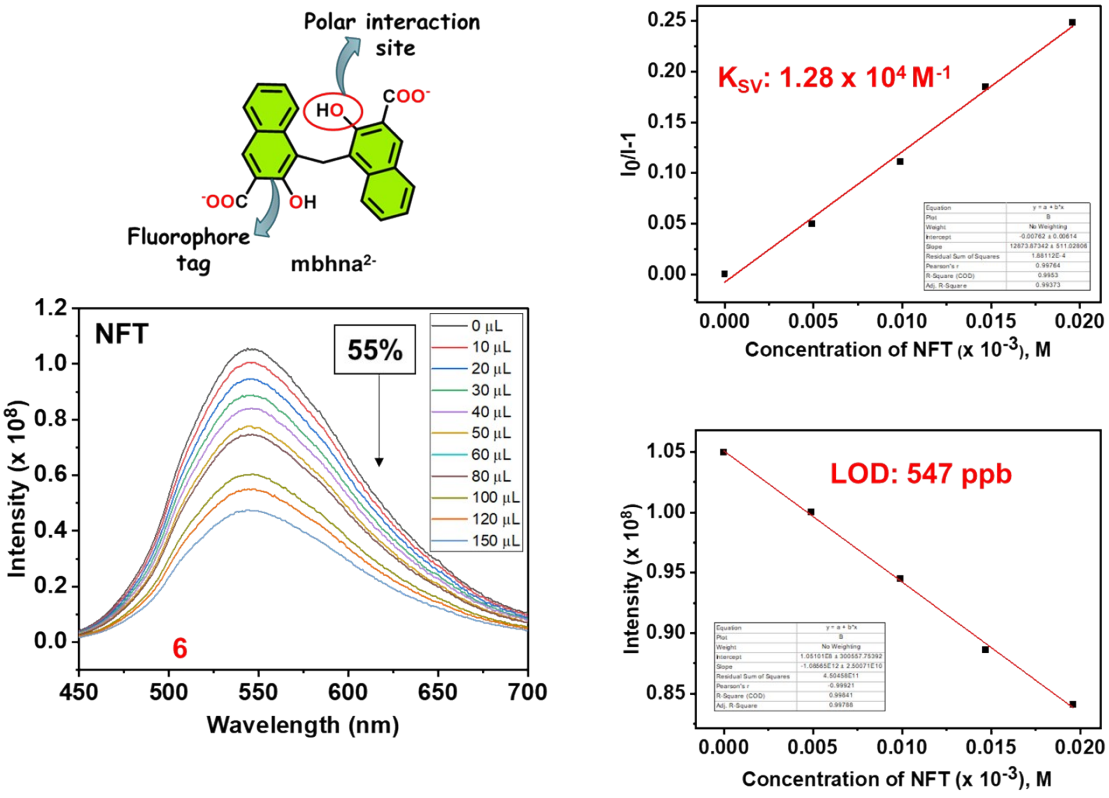

Fig. S35 Fluorescence based detection of NFT by **6**.

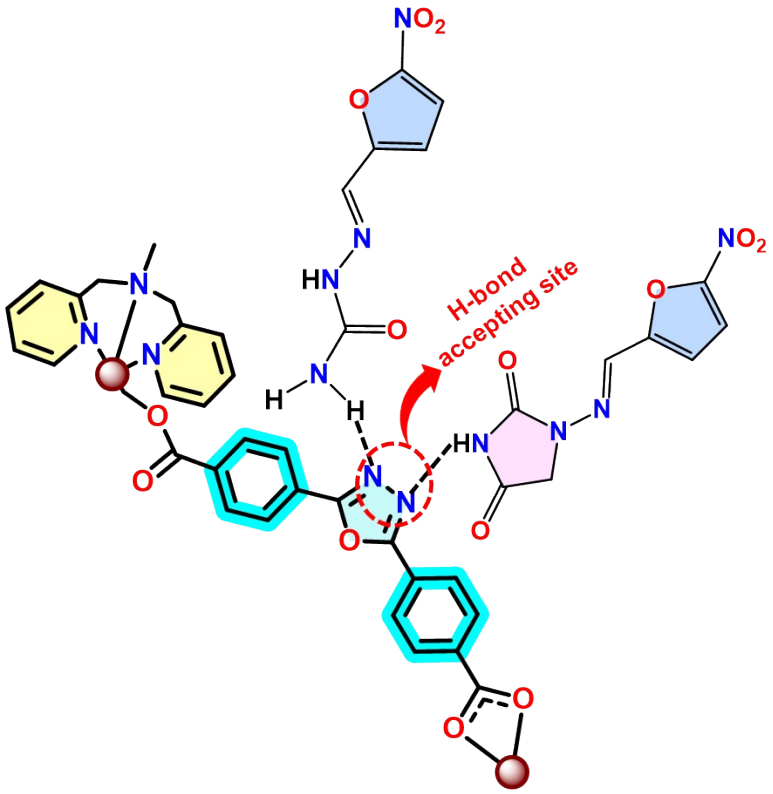

Fig. S36 Interaction of NFT and NFZ with compound **4** through H-bond.

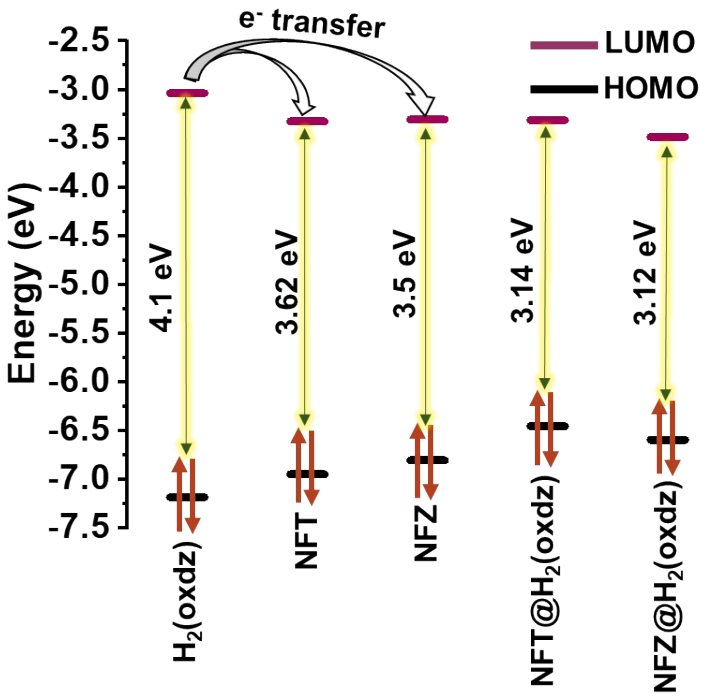

Fig. S37 HOMO−LUMO energy levels of the H_2(oxdz), NFT and NFZ, and rearranged HOMO-LUMO energy levels of NFT@H_2(oxdz) and NFZ@H_2(oxdz) after electron transfer determined by DFT calculations using B3LYP at the 6-31G (d,p) basis set of the Gaussian 09 program.

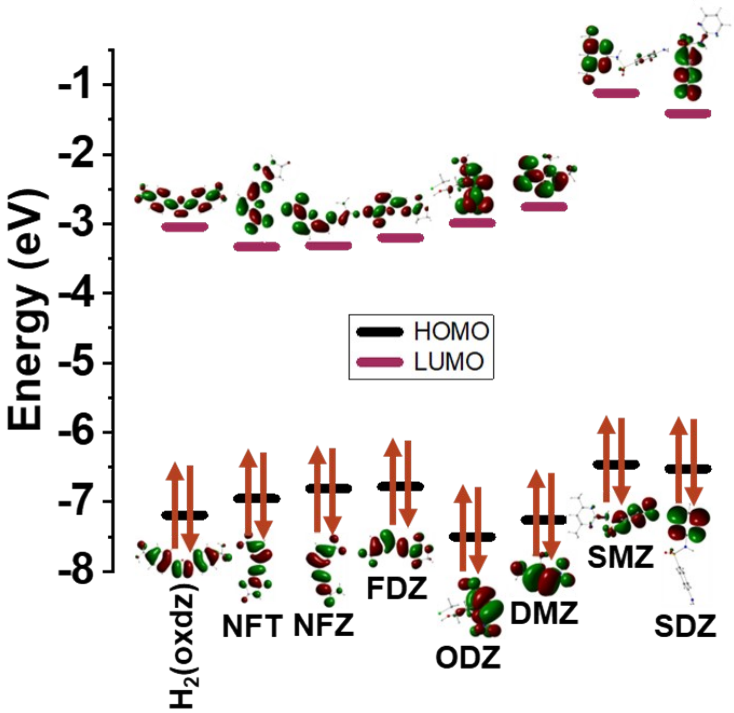

Fig. S38 HOMO−LUMO energy levels of the H_2(oxdz) along with different antibiotics determined by DFT calculations using B3LYP at the 6-31G (d,p) basis set of the Gaussian 09 program.

Table S1. Crystallographic Data and Structure Refinement Parameters for **2**, **3** and **4**

compound	**2**	**3**	**4**
chemical formula	$C_{29}H_{25}N_5NiO_6$	$C_{29}H_{23}N_5O_5Zn$	$C_{29}H_{23}CdN_5O_5$
formula weight (g/mol)	598.25	586.932	633.948
temperature (K)	296(2)	296.15	296.15
radiation	Mo Kα	Mo Kα	Mo Kα
wavelength (Å)	0.71073	0.71073	0.71073
crystal system	orthorhombic	monoclinic	orthorhombic
space group	*Pnma*	$P2_1/c$	*Pbcn*
a (Å)	8.612(2)	8.8119(5)	22.705(4)
b (Å)	17.731(4)	16.0391(10)	29.041(3)
c (Å)	17.677(5)	24.3538(17)	9.3707(12)
a (°)	90	90	90
b (°)	90	91.353(4)	90
g (°)	90	90	90
Z	4	4	8
V ($Å^3$)	2699.3(12)	3441.1(4)	6178.6(14)
density (g/cm^3)	1.472	1.133	1.363
μ (mm^{-1})	0.772	0.752	0.751
F(000)	1240	1210.2	2555.2
theta (°) range for data coll.	2.871 to 25.127	1.52 to 25.43	2.28 to 25.01
reflections collected	9167	23268	20575
independent reflections	2462	6328	5400
Reflections with $I > 2\sigma(I)$	2128	4303	3673
R_{int}	0.0363	0.0607	0.0723
no. of parameters refined	201	361	357
GOF on F^2	1.024	0.9666	1.031
final $R_1{}^a/wR_2{}^b$ ($I > 2\sigma(I)$)	0.0303/0.0720	0.0600/0.1716	0.0709/0.1319
$R_1{}^a/wR_2{}^b$ (all data)	0.0371/0.0758	0.0870/0.1904	0.1014/0.1427
largest diff. peak and hole ($eÅ^{-3}$)	0.25 and -0.37	0.86 and -0.93	1.47 and -0.1.61

$^{a}R_1 = \Sigma||F_o| - |F_c||/\Sigma|F_o|$. $^{b}wR_2 = [\Sigma w(F_o^2 - F_c^2)^2/\Sigma w(F_o^2)^2]^{1/2}$, where $w = 1/[\sigma^2(F_o^2) + (aP)^2 + bP]$, $P = (F_o^2 + 2F_c^2)/3$

Table S2. Comparison of detection of NFT by MOCNs reported in the literature

Analyte (NFT)	**K_{sv} (M^{-1})**	**LOD**	**Reference**
$\{[Cd(oxdz)(bpma)]\cdot 4H_2O\}_n$ **(4)**	6.77 x 10^4	197 ppb or 0.831 μmol/L	**This work**
$\{[Zn_2(4\text{-tpom})_2(oxdz)_2]\cdot H_2O\}_n$	6.55 x 10^4	89 ppb	S7
BUT-12 BUT-13	3.8 x 10^4 6 x 10^4	-	S8
$\{[Eu_2(BCA)_3(H_2O)(DMF)_3]\cdot 0.5DMF\cdot H_2O\}_n$	1.6 x 10^4	0.21 μM	S9
$[Mg_2(APDA)_2(H_2O)_3]\cdot 5DMA\cdot 5H_2O$	8.82 x 10^4	126 ppb	S10
$\{[In\text{-}(BTDI)]\cdot Me_2NH_2\cdot 2H_2O$ (In-BTDI)	4.7 x 10^4	202 ppb	S11
$\{[Tb\text{-}(HL)(H_2O)_2]\cdot x(solv)\}_n$ H_4L: 5,5′-(((1,4-phenylenebis-(azanediyl))bis(carbonyl))bis(azanediyl))diisophthalic acid	1.9 x 10^4	0.41 μM	S12
$[Zn_2(azdc)_2(dpta)]\cdot(DMF)_4$ (CSMCRI-2)	7.14 x 10^4	-	S13
$[Zn_8(C_5H_4N_5)_4(C_{14}H_8O_4)_6O(C_{50}H_{44}N_4)_{0.5}]$	4.42 x 10^4	133 ppb	S14

ZTMOF-1	7.055×10^4	0.175 µM	S15
$\{[Zn_3(TCPPDA)_4]\cdot 8DMF \cdot 2H_2O\}_n$ (ZJU-126)	4×10^4	0.82 µM	S16
$[TbL\cdot 2H_2O]_n$	5.26×10^4	826 ppb	S17
RhB@ZIF-8 FSS@ZIF-8	1.8×10^4 2×10^4	0.26 µM 0.31 µM	S18
$\{[Eu(H_2O)(BTCTB)]\cdot 2H_2O\}_n$	2.1×10^4	0.60 µM	S19
Eu-MOF	2.39×10^5	0.38 µM	S20
$[Eu(bcbp)(tdc)(H_2O)_3]\cdot Cl\cdot 5H_2O$	2.24×10^3	2.80 µM	S21
[Zn(TTDPa) (bodca)·H_2O [Zn(TTDPb) (bodca)·H_2O	5.94×10^4 8.59×10^4	0.975 µM 0.285 µM	S22
$[Cd_3(TDCPB)\cdot 2DMAc]\cdot DMAc\cdot 4H_2O$	1.04×10^5	-	S23
$[Tb(TATMA)(H_2O)\cdot 2H_2O\}n$	3×10^4	-	S24
$[Zn_3(bpg)_{1.5}(azdc)_3]\cdot(DMF)_{5.9}\cdot(H_2O)_{1.05}$ (CSMCRI-1)	5.92×10^4	-	S25
$[Cd_2Cl(L)(H_2O)]\cdot 11H_2O$ (L^{3-} = 2,4,6-tris(1-(3,5-dicarboxylatobenzyl)pyridinium4-yl)pyridine	1.5×10^4	0.26 µM	S26
[Eu(cppa)(OH)]·xS (CTGU-19)	2.33×10^4	0.43 µM	S27
$[Cd_3\cdot L\cdot(BTB)_2\cdot 2DMF]$ (CUST-532) $[(Cd_3O_2)\cdot L\cdot BTC]$ (CUST-533) L = 9,10-bis(N-benzimidazolyl)-anthracene	6.81×10^4 3.80×10^4	0.44 µM 0.78 µM	S28
RhB@Tb-dcpcpt Tb-dcpcpt : $[Tb_3(dcpcpt)_3(HCOO)]\cdot DMF\cdot 15H_2O$	4.53×10^4	158 ppb	S29
$\{[Tb_2(AIP)_2(H_2O)_{10}]\cdot(AIP)\cdot 4H_2O\}_n$	4×10^4	0.30 µM	S30
$[(Zn_4O)_2(PDDA)_6(H_2O)_2]\cdot 10DMF$	1.16×10^5	-	S31
$[Cd(MBPz)(2,6\text{-}NDC)]\cdot 2H_2O\}_n$ (IITKGP-71)	2.1×10^4	0.17 µM	S32
$\{[Eu_2(H_2O)L_3]\cdot 3H_2O\}_n$ H_2L =1,2,5-thiadiazole-3,4-dicarboxylicacid	1.52×10^4	0.97 µM	S33

Table S3. Comparison of detection of NFZ by MOCNs reported in the literature

Analyte (NFZ)	K_{sv} (M^{-1})	LOD	Reference
$\{[Cd(oxdz)(bpma)]\cdot 4H_2O\}_n$ **(4)**	5.86×10^4	172 ppb or 0.869 µmol/L	**This work**
$\{[Zn_2(4\text{-tpom})_2(oxdz)_2]\cdot H_2O\}_n$	4×10^4	78 ppb	S7
BUT-12 BUT-13	1.1×10^5 7.5×10^4	58 ppb 90 ppb	S8
$\{[Eu_2(BCA)_3(H_2O)(DMF)_3]\cdot 0.5DMF\cdot H_2O\}_n$	2.2×10^4	0.16 µM	S9
$[Zn_2(azdc)_2(dpta)]\cdot(DMF)_4$ (CSMCRI-2)	1.30×10^5	630 ppb	S13
$[Zn_8(C_5H_4N_5)_4(C_{14}H_8O_4)_6O(C_{50}H_{44}N_4)_{0.5}]$	4.48×10^4	110 ppb	S14
$\{[Zn_3(TCPPDA)_4]\cdot 8DMF\cdot 2H_2O\}_n$ (ZJU-126)	5.8×10^4	0.56 µM	S16
RhB@ZIF-8 FSS@ZIF-8	7.3×10^4 8×10^4	0.47 µM 0.35 µM	S18
$\{[Eu(H_2O)(BTCTB)]\cdot 2H_2O\}_n$	1.27×10^4	0.67 µM	S19
Eu-MOF	2.20×10^5	0.41 µM	S20
$[Eu(bcbp)(tdc)(H_2O)_3]\cdot Cl\cdot 5H_2O$	6.41×10^3	1.33 µM	S21
[Zn(TTDPa)(bodca).H_2O [Zn(TTDPb) (bodca).H_2O	6.76×10^4 1.12×10^5	0.857 µM 0.218 µM	S22
$[Cd_3(TDCPB)\cdot 2DMAc]\cdot DMAc\cdot 4H_2O$	7.46×10^4	-	S23
$\{[Tb(TATMA)(H_2O)\cdot 2H_2O\}_n$	3.35×10^4	-	S24
$[Zn_3(bpg)_{1.5}(azdc)_3]\cdot(DMF)_{5.9}\cdot(H_2O)_{1.05}$ CSMCRI-1	8.75×10^4	0.8 ppm	S25
$[Cd_2Cl(L)(H_2O)]\cdot 11H_2O$ (L^{3-} = 2,4,6-tris(1-(3,5-dicarboxylatobenzyl)pyridinium4-yl)pyridine	2.1×10^4	0.20 µM	S26
RhB@Tb-dcpcpt Tb-dcpcpt: $[Tb_3(dcpcpt)_3(HCOO)]\cdot DMF\cdot 15H_2O$	4.45×10^4	134 ppb	S29
$\{[Tb_2(AIP)_2(H_2O)_{10}]\cdot(AIP)\cdot 4H_2O\}_n$	2.8×10^4	0.35 µM	S30
$[(Zn_4O)_2(PDDA)_6(H_2O)_2]\cdot 10DMF$	6.08×10^4	-	S31
$[Cd(MBPz)(2,6\text{-NDC})]\cdot 2H_2O\}_n$ (IITKGP-71)	3.1×10^4	0.11 µM	S32
$\{[Eu_2(H_2O)L_3]\cdot 3H_2O\}_n$ H_2L =1,2,5-thiadiazole-3,4-dicarboxylicacid	2.82×10^4	0.52 µM	S33
$[Zn_4O(BCTPE)_3]$	-	0.1 ppm	S34

Table S4. Average lifetime values of **4** before and after addition of different volumes of nitrofurans

Probe	Average lifetime before addition of analyte (ns)	Average lifetime after addition of 50 µL of analyte (ns)	Average lifetime after addition of 100 µL of analyte (ns)	Average lifetime after addition of 150 µL of analyte (ns)	Nature of quenching
4 (NFT)	0.121	0.121	0.113	0.09	Static and dynamic
4 (NFZ)	0.121	0.107	0.108	0.102	Static and dynamic

Table S5. HOMO and LUMO energies calculation for H_2(oxdz), antibiotics, NFT@H_2(oxdz), and NFZ@H_2(oxdz) using B3LYP/6-31G(d,p) level

Compound	HOMO (eV)	LUMO (eV)	Band Gap (eV)
H_2(oxdz)	-7.19	-3.04	4.1
NFT	-6.954	-3.33	3.62
NFZ	-6.81	-3.31	3.5
FDZ	-6.7797	-3.20	3.57
ODZ	-7.5	-2.991	4.51
DMZ	-7.26	-2.757	4.5
SMZ	-6.459	-1.1197	5.33
SDZ	-6.523	-1.41	5.113
NFT@H_2(oxdz)	-6.46	-3.317	3.14
NFZ@H_2(oxdz)	-6.60	-3.4879	3.12

References

[S1] APEX2, SADABS, and SAINT, Bruker AXS Inc., Madison, WI, USA, 2008.
[S2] G. M. Sheldrick, *Acta Crystallogr., Sect. A: Found. Crystallogr.*, 2008, **64**, 112–122.
[S3] O. V. Dolomanov, L. J. Bourhis, R. J. Gildea, J. A. K. Howard and H. Puschmann, *J. Appl. Cryst.*, 2009, **42**, 339–341.
[S4] C. F. Macrae, I. J. Bruno, J. A. Chisholm, P. R. Edgington, P. McCabe, L. Monge, R. Taylor, J. van de Streek and P. A. Wood, *J. Appl. Crystallogr.*, 2008, **41**, 466–470.
[S5] K. Brandenburg, H. Putz, M. Berndt, *DIAMOND V 3.2* Crystal Impact GbR, Bonn, Germany, 1999.
[S6] M. J. Frisch, G. W. Trucks, H. B. Schlegel, G. E. Scuseria, M. A. Robb, J. R. Cheeseman, G. Scalmani, V. Barone, B. Mennucci, G. A. Petersson, H. Nakatsuji, M. Caricato, X. Li, H. P. Hratchian, A. F. Izmaylov, J. Bloino, G. Zheng, J. L. Sonnenberg, M. Hada, M. Ehara, K. Toyota, R. Fukuda, J. Hasegawa, M. Ishida, T. Nakajima, Y. Honda, O. Kitao, H. Nakai, T. Vreven, J. A. Montgomery Jr., J. E. Peralta, F. Ogliaro, M. Bearpark, K. N. Kudin, V. N. Staroverov, T. Keith, R. Kobayashi, J. Normand, K. Raghavachari, A. Rendell, J. C. Burant, S. S. Iyengar, J. Tomasi, M. Cossi, N. Rega, J. M. Millam, M. Klene, J. E. Knox, J. B. Cross, V. Bakken, C. Adamo, J. Jaramillo, R. Gomperts, R. E. Stratmann, O. Yazyev, A. J. Austin, R. Cammi, C. Pomelli, J. W. Ochterski, R. L. Martin, K. Morokuma, V. G. Zakrzewski, G. A. Voth, P. Salvador, J. J. Dannenberg, S. Dapprich, A. D. Daniels, O. Farkas, J. B. Foresman, J. V. Ortiz, J. Cioslowski and D. J. Fox, *Gaussian 09*, Gaussian, Inc., Wallingford CT, 2013.
[S7] A. Chanda and S. K. Mandal, *Chem. Asian J.*, 2025, **20**, e202401206.
[S8] B. Wang, X.-L. Lv, D. Feng, L.-H. Xie, J. Zhang, M. Li, Y. Xie, J. Li and H.-C. Zhou, *J. Am. Chem. Soc.*, 2016, **138**, 6204–6216.
[S9] F. Zhang, H. Yao, T. Chu, G. Zhang, Y. Wang and Y. Yang, *Chem. Eur. J.*, 2017, **23**, 10293–10300.
[S10] N. Xu, Q. Zhang, B. Hou, Q. Cheng and G. Zhang, *Inorg. Chem.*, 2018, **57**, 13330–13340.
[S11] Z. Zhang, Z. Wu, Z. Li, Y. Zhao, M. Yu, F. Jiang, L. Cheng and M. Hong, *Cryst. Growth Des.*, 2023, **23**, 4491–4498.
[S12] M. Lei, F. Ge, X. Gao, Z. Shi and H. Zheng, *Inorg. Chem.*, 2021, **60**, 10513–10521.
[S13] R. Goswami, S. C. Mandal, N. Seal, B. Pathak and S. Neogi, *J. Mater. Chem. A*, 2019, **7**,

19471–19484.
[S14] Y.-M. Ying, C.-L. Tao, M. Yu, Y. Xiong, C.-R. Guo, X.-G. Liu and Z. Zhao, *J. Mater. Chem. C*, 2019, **7**, 8383–8388.
[S15] H. Li, J. Ren, X. Xu, L. Ning, R. Tong, Y. Song, S. Liao, W. Gu and X. Liu, *Analyst*, 2019, **144**, 4513–4519.
[S16] M. Lu, X. Xiao, S. Yu, W. Lin and Y. Yang, *Z. Anorg. Allg. Chem.*, 2022, **648**, e202100353.
[S17] F. Guo, C. Su, Y. Fan and W. Shi, *Dalton Trans.*, 2019, **48**, 12910–12917.
[S18] Y.-Q. Zhang, X.-H. Wu, S. Mao, W.-Q. Tao and Z. Li, *Talanta*, 2019, **204**, 344–352.
[S19] H.-W. Yang, P. Xu, B. Ding, Z.-Y. Liu, X.-J. Zhao and E.-C. Yang, *Eur. J. Inorg. Chem.*, 2019, **2019**, 5077–5084.
[S20] Y. Su, Y. Guo, Q. Wu, L. Wang, Y. Wang, G. Yang, W. Zhang and Y. Wang, *Inorg. Chem.*, 2024, **63**, 15134–15143.
[S21] X. Li, S. Zhang, L. Zhang, Y. Yang, K. Zhang, Y. Cai, Y. Xu, Y. Gai and K. Xiong, *Cryst. Growth Des.*, 2022, **22**, 3991–3997.
[S22] Z.-L. Mu, Y.-Q. Ma, Y. Zhu, Z. Chen, H.-P. Xiao, X. Li, H.-Y. Wang and J.-Y. Ge, *Inorg. Chem.*, 2023, **62**, 20314–20324.
[S23] Q.-Q. Zhu, Q.-S. Zhou, H.-W. Zhang, W.-W. Zhang, D.-Q. Lu, M.-T. Guo, Y. Yuan, F. Sun and H. He, *Inorg. Chem.*, 2020, **59**, 1323–1331.
[S24] Q.-Q. Zhu, H. He, Y. Yan, J. Yuan, D.-Q. Lu, D.-Y. Zhang, F. Sun and G. Zhu, *Inorg. Chem.*, 2019, **58**, 7746–7753.
[S25] R. Goswami, S. C. Mandal, B. Pathak and S. Neogi, *ACS Appl. Mater. Interfaces*, 2019, **11**, 9042–9053.
[S26] P. Li, M.-Y. Guo, L.-L. Gao, X.-M. Yin, S.-L. Yang, R. Bu and E.-Q. Gao, *Dalton Trans.*, 2020, **49**, 7488–7495.
[S27] B. Li, Y.-Y. Jiang, Y.-Y. Sun, Y.-J. Wang, M.-L. Han, Y.-P. Wu, L.-F. Ma and D.-S. Li, *Dalton Trans.*, 2020, **49**, 14854–14862.
[S28] M. Fan, B. Sun, X. Li, Q. Pan, J. Sun, P. Ma and Z. Su, *Inorg. Chem.*, 2021, **60**, 9148–9156.
[S29] M. Yu, Y. Xie, X. Wang, Y. Li and G. Li, *ACS Appl. Mater. Interfaces*, 2019, **11**, 21201–21210.
[S30] F. Zhang, H. Yao, Y. Zhao, X. Li, G. Zhang and Y. Yang, *Talanta*, 2017, **174**, 660–666.
[S31] H. He, Q.-Q. Zhu, M.-T. Guo, Q.-S. Zhou, J. Chen, C.-P. Li and M. Du, *Cryst. Growth Des.*, 2019, **19**, 5228–5236.
[S32] S. Mondal, R. Sahoo and M. C. Das, *Small*, 2025, **21**, 2409095.
[S33] X. Yu, D. I. Pavlov, A. A. Ryadun, K. A. Kovalenko, A. S. Potapov and V. P. Fedin, *Inorg. Chem*., 2025, **64**, 6356–6364.
[S34] X.-G. Liu, C.-L. Tao, H.-Q. Yu, B. Chen, Z. Liu, G.-P. Zhu, Z. Zhao, L. Shen and B. Z. Tang, *J. Mater. Chem. C*, 2018, **6**, 2983–2988.